Acta Geochim (2022) 41(5):861–886
https://doi.org/10.1007/s11631-022-00552-z

ORIGINAL ARTICLE

Geochemical evaluation of mineralization potential of the Somie-Ntem area within the Tikar plain, Cameroon: implication on petrogenesis

Mero Yannah[1] · Yaya Fodoué[1] · Maurice Kwékam[2] · Benoit Joseph Mbassa[1] · Juliana Amboh Tifang[1] · Armand Dongmo Kagou[2] · Samuel Ndonwi Ayonghe[3]

Received: 3 December 2021 / Revised: 1 June 2022 / Accepted: 5 June 2022 / Published online: 11 July 2022

Abstract Somie-Ntem area of the Tikar plain belongs to the western Cameroon Domain. The lithology of the plain has been characterized, and the mineral potential is still unclear despite previous reports on Sn deposit within one of the magmatic complexes. Our results show two groups of granitic rocks displaying oxidized and reduced character; (1) mesocratic (oxidized) granites including biotite-bearing, hornblende-biotite-bearing, hornblende-epidote-bearing and pyroxene-bearing; (2) leucogranites (reduced) that are generally amphibole-pyroxene bearing. These granitoids are hosted by gneisses and metasedimentary rocks partially covered by rhyolites. Major element composition shows high-K calc-alkaline to shoshonite affinity, metaluminous to weakly peraluminous I-type granites. Mesocratic granites show moderately negative Eu anomaly, depleted in Nb, P, Ti, and are related to syn-collisional setting. Leucogranites are post-orogenic with strong negative Eu anomaly, depleted in Ba and Sr and enriched in Hf, Nb and Ta. They are fertile in Sn and Zn, enriched through postmagmatic metasomatism and greisenization. Cr–Cu–Ni–V mineralization occurs in hornblende-bearing gneisses and their enrichment suggests a possible Ni–Cu-type PGEs mineralization in this area. Meanwhile, their trace element shows high Ni/Cu, very low Rb/Sr, low LILE and LREE which indicates mantle fractionation at subduction. The absence of olivine and pyroxene, and increased SiO_2 and Al_2O_3 in the Cr–Cu–Ni–V-bearing rocks show that the parent magma experienced fractional crystallization and crustal contamination during evolution. Notwithstanding, the high Zr/Rb and K/Rb ratios show that hydrothermal activity was not intense to enhance mineralization in the area. Variation in the direction of stress during shear deformation inhibited an effective hydrothermal activity and ore deposition in the region.

Keywords Geochemistry · Mineralization · Somie-Ntem · Tikar plain · Cameroon

✉ Mero Yannah
merotumi@gmail.com

1 Institute of Geological and Mining Research, Yaounde, Cameroon

2 Department of Earth Sciences, University of Dschang, Dschang, Cameroon

3 Central Unit for Internal Control and Evaluation, University of Buea, Buea, Cameroon

1 Introduction

The economic growth of a nation depends partly on the exploration of its natural resources. Keeping aside water, forest and other natural resources, mineral exploitation, and production are essential to industrial and economic development (e.g. Matos et al. 2012). South American and the African blocks have shown significant litho-structural similarities since the breaking of the Gondwana supercontinent (Trompette 1994). Pan-African orogenic event emplaces a series of granitoids, metavolcanics and volcano sedimentary rocks across the two continents alongside major shear zone known in Cameroon and Brazil as the Central Cameroon Shear Zone (CCSZ, Ngako et al. 2003) and Brasiliano shear zone (Neves et al. 2002) respectively. Nevertheless, Pan-African basement of the Tikar plain has locally host several mineralization in several zones within the west and central African sub regions (Markwitz et al. 2016), including gold in the greenstone belt in Ghana (Grenholm 2011), massive sulphide ores in Kabwe and Tsumeb belts of Zambia and Namibia respectively (Chetty and Frimmel 2000). In Cameroon, these granitoids host gold and uranium in eastern (Suh et al. 2006) and northern (Kouske et al. 2012) part of the country, respectively. Some of the mineralizations are associated with fluid conduits in the form of dykes, lode, veins (Rhys et al. 2003; Suh et al. 2006; Duuring et al. 2009; Bambi et al. 2012; Yannah et al. 2015). Previous studies show that the worlds' ore elements deposits, including major (Mn, Sn, W, Ta, Nb, Zr, Zn, Au, U) and minor (Sc, Sb, Bi and Cd) elements are related to granitoids (Sillitoe 1996). Amongst these, I-type calc-alkaline magmas are efficient in the concentration of base metals like Fe, Cu, Cr, Mo, while evolved S-type granites are associated with Sn and W (Ghodsi et al. 2016). The regional geology of Cameroon shows the vast distribution of granitoid rocks within the west, the north and central-east regions (Toteu et al. 2001). Even though they have been proven to be Pan-African, work is still ongoing to know more about their origin, evolution trajectory and mineralization. Most works have been able to characterize, correlate and date lithologies in different environments within the Western Cameroon Domain (WCD), Adamawa-Yadé Domain (AYD) and the Southern Cameroon Domain (SCD) of the Cameroon Pan-African belt (Ngako et al. 2008; Tetsopgang et al. 2006; Nzenti et al. 2010, 2017; Kouankap Nono et al. 2013, 2018; Yap et al. 2018). Evaluating primary mineralization in geological formations is very uncommon within the WCD in general and Tikar plain in particular, except for recent work on the Mbengwi granitoids (Mbassa et al. 2018), Mayo Salah plutons (Tchunte et al. 2018) and Misajé I-type granite plutons (Fozing et al. 2021). The study area is located within the Tikar plain, which is part of the WCD where no exploration or mining activities are happening in spite of some reports on tin (Sn) mineralization (Nguéné 1982) in one of the complexes. There is a general problem faced by the mining sector in Cameroon in the sense that explorers are mostly guided by artisanal miners whose interest is in alluvial deposits (secondary mineralization). This has prompted recent works to show interest in investigating primary mineralization within lithologies. The main purpose of this paper is to study the different rock types in the Somie-Ntem area from whole-rock geochemistry in order to identify their mineralization potentials and decipher their petrogenetic constrains. This will contribute to the understanding of the geodynamic and magmatic evolution along the tectonic corridor.

2 Geological setting

The Pan-African orogeny forms an integral part of Cameroon geology. This orogenic belt that covers the study area is also known as the Pan-African Belt of Central Africa (Penaye et al. 1993) or Central African Fold Belt. It constitutes an association of the Sao-Francisco Craton, Congo Craton, Eastern Saharan Block and the West African Craton (Ngako and Njonfang 2011). This fold belt marks a major Neoproterozoic connection between the Trans-Saharan belt of West Africa and the Brazilliano orogenic belt in NE Brazil (Toteu et al. 2001; Ngako and Njonfang 2011). In Cameroon, the CAFB is partitioned into southern, central and northern Cameroon domains of geotectonic units (Ngako et al. 2008).

The Northern Cameroon Domain (NCD) (Fig. 1b), also known as the WCD (West Cameroon Domain) (Toteu et al. 2004) or the Poli Group (Ngako et al. 2008) falls north of the Tchollire-Banyo shear zone (TBSZ), (Toteu et al. 2001, 2004) and marked by: (1) back-arc basin formation (Toteu 1990; Montes-Lauar et al. 1997; Ngako 1999), characterized by pre- to syn-tectonic calc-alkaline basic to intermediate orthogneisses and granitoids dated 740–630 Ma relating to subduction zone (Toteu et al. 1987, 2001); (2) late- to post-collisional intrusions (from 620 to 580 Ma) associated with shearing and migmatization (Toteu et al. 2001; Tchameni et al. 2016; Negue et al. 2017) and; (3) mafic and felsic post tectonic alkaline granitoids (550–530 Ma) related to crustal extension (Toteu et al. 1986, 2004; Dawai et al. 2013); (4) Neoproterozoic medium to high-grade gneisses and schists having volcano-sedimentary and volcanic origin. According to some studies, Pan-African granitoids of the WCD originated from a juvenile crust or intensive reworking of the Paleoproterozoic crust (Toteu et al. 2001, 2004). Within the WCD, these granitoids display similarities in composition (Djouka-Foukwé et al. 2008; Tetsopgang et al. 2006). However, their whole-rock geochemistry generally indicates high-K calc-alkaline to shoshonite magmatism of I-type with few S and A-type origin (Ngo-Beloun et al. 2006; Djouka-Fonkwé et al. 2008; Nzina et al. 2010; Kwékam et al. 2020b, c; Fozing et al. 2021).

The Somi-Ntem area of the Tikar Plain lies north of the Tchollie-Banyo Shear Zone (TBSZ). This shear zone separates the WCD from the AYD (Toteu et al. 2001). Structures within the WCD are linked to three deformation phases denoted D_1 to D_3 (Nzenti et al. 1992; Toteu et al. 2001, 2004). These include flat-lying foliations associated with isoclinal folds (Ngako et al. 1992; Nzenti et al. 1992) interpreted as D_1 (Toteu et al. 2001), and are related to the nappe type tectonics of the Pan-African (Ferré et al. 1996). D_2 structures include tight and upright folds with vertical axial plane foliations (Toteu et al. 2004; Ngako et al. 2008) displaying sinistral movement that shows parallelism to the Sanaga Fault (SF) while D_3 forms a late tectonic dextral event that characterized most part of the CCSZ (Ngako et al. 2003, 2008). In general, tectonic evolution transgresses from D_2-D_3 displaying sinistral to dextral

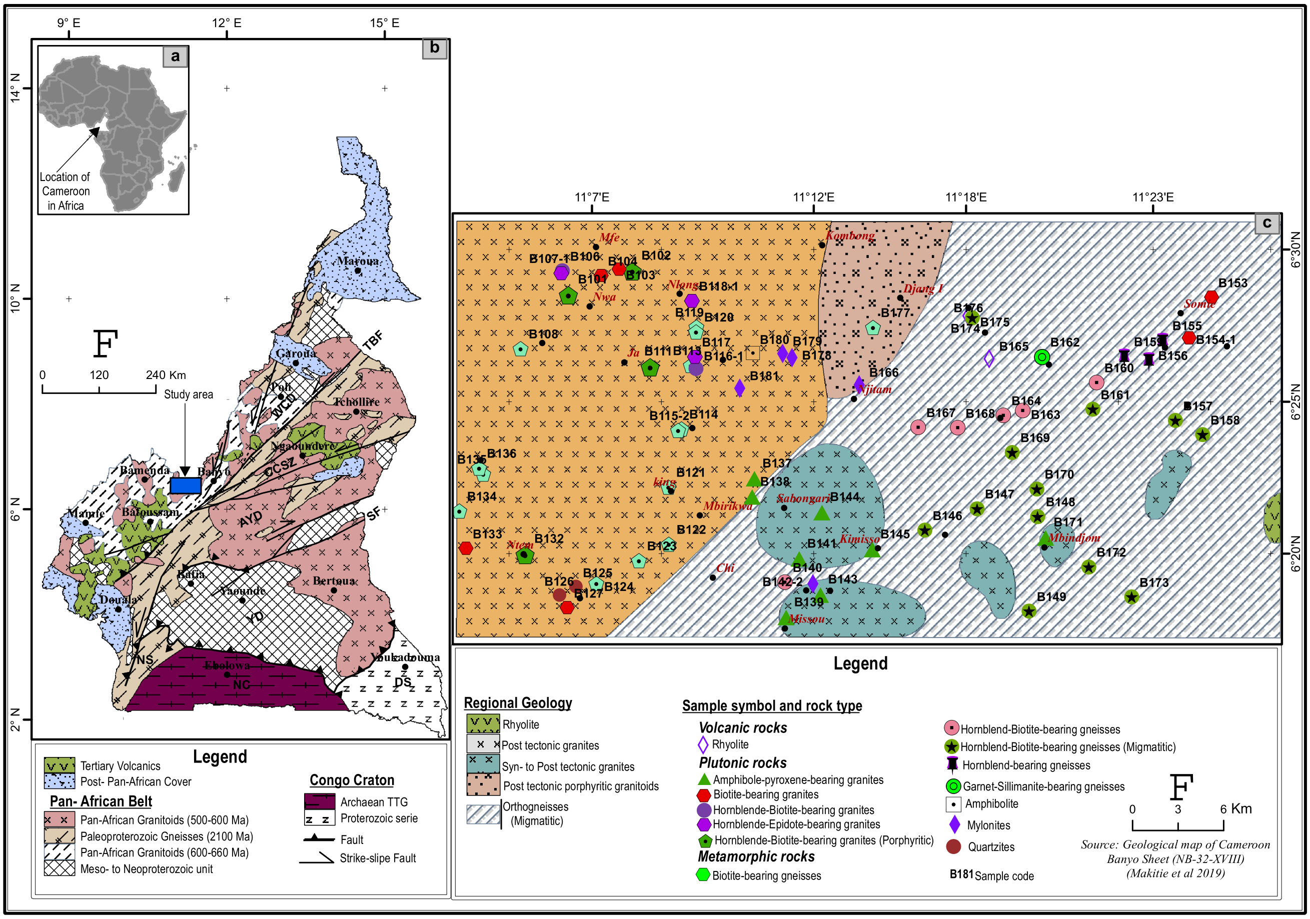

Fig. 1 Location of the study area. **a** Cameroon in Africa; **b** Cameroon regional geologic map indicating major geotectonic units and older formations (Toteu et al. 2001; Ngako et al. 2008; Njanko et al. 2010) 1-Yaounde Domain (YD), 2-Adamawa-Yadé Domain (AYD), 3-Western Cameroon Domain (WCD), NS-Nyong series, NC-Ntem complex, DS-Dja series; major faults and shear zones: AF-Adamawa fault; TBF-Tchollirè-Banyo fault; SF-Sanaga fault; CCSZ-Cantral Cameroon Shear Zone; **c** study area showing regional geology (adopted from Le Marechal 1975; Makitie et al. 2019) with overlayed sample points of different lithologies identified during this study

movements respectively (Toteu et al. 2004; Yakeu et al. 2007; Ngako et al. 2008; Njanko et al. 2010), with D_1 and D_2 events dominating within the WCD and AYD (Toteu et al. 1991, 2004; Ngako et al. 1992; Nzenti et al. 1992; Ferré et al. 1996).

3 Materials and methods

During the field work, a total of 81 sample locations were observed (Fig. 1c) and amongst them, 30 representative rock samples were selected for geochemical and petrographical analysis. These include orthogneisses, paragneisses, mesocratic granites, leucogranites, and rhyolite. The criteria for the selection of these samples were based on field observations and the cost of analyses. As indicated in the sample location map, each rock type observed on the field have a representative sample(s) selected for laboratory analysis (Fig. 1c). For the petrographic study, 30 polished thin sections were prepared at the Laboratory of the University of Johannesburg in South Africa for detailed analysis of the mineralogical and textural aspects of the rocks. Replicates of the 30 samples were used for whole-rock geochemical analysis. At the Activation Laboratories (ActLabs) of Ontario Canada, the geochemical samples were entirely pulverized to a nominal $-$ 2 mm mesh fraction and mechanically split to obtain a representative sample. 250 g of each sample pulverized was brought to 95%, $-$105 µm grain size. Sample powders were further inserted into an Inductive Coupled Plasma Mass Spectrometer (ICP-MS) for elemental analysis. This followed a method known as 4Litho which is a combined whole-rock ICP-OES and trace elements ICP-MS packages into a Lithium Metaborate and Tetraborate Fusion—ICP and ICP-MS. With this method, the fused sample was diluted and analyzed using Perkin Elmer or 9000 ICP-MS. The detection limit of 0.01% was set for the major elements except for MnO and TiO_2 with 0.001%. For the trace elements, the detection limit was set at 2 ppm except for Zn Ni and Cr at 20 ppm, while Pb, As and V was 5 ppm. Geochemical interpretation diagrams and graphical representation were done using GCDkits software by Janoušek et al. (2006).

Positive anomalies in the dataset were determined from the distribution of the data on statistical box plots and histograms. On the box plot, the line in the middle of the box is the median or the 50-percentile given as $Q_2 = 50\%$. The first (Q_1) and third (Q_3) quartiles are 25% and 75%, respectively, and representing the lower and upper percentiles. Meanwhile, the difference between Q_1 and Q_3 is known as the interquartile range (IQR), indicating the extreme values calculated from a window of 1.5 IQR. The statistical threshold for the element concentration was calculated using the formula given as follows: Threshold = $Q_3 + 1.5$ (IQR) for the upper cutoff threshold (Dekking et al. 2005). Values above the threshold are outliers and represent positive anomalies and possible mineralization.

4 Results

4.1 Petrography

Petrographic of the Somie-Ntem lithologies is well described in Yannah (2020). The results show the distribution of different lithologies within the Somie-Ntem area more than what is observed from the regional geological map (Fig. 1b). This area is hosted by a metamorphic basement characterized by both para and orthoderived gneisses. These paragneisses show bands of aligned biotite, garnet and sillimanite forming a smooth cleavage domain with spaced schistosity. Garnet crystals form porphyroblasts within the mafic bands while sillimanite is confined within the felsic bands. Quartz, plagioclase, and orthoclase are also present with titanite, epidote and zircon as accessories. The orthoderived rocks outcrop within the valleys, forming bedrocks and enclaves within granites. They also form small massifs on the eastern corner of the study area. The rocks vary in composition from biotite-bearing, hornblende-biotite-bearing, hornblende-bearing and amphibolites, with the hornblende-bearing and amphibolites making the mafic group. The hornblende-biotite gneisses are commonly migmatitic and mylonitic. Micro-texture show grain boundaries that vary from amoeboid, inequigranular to seriate interbolate. Foliations are generally discrete to continuous with spaced schistosity defined by the preferred orientation of biotite mineral (Fig. 2a–f). The cleavage domain is rough, with dark phase minerals making about 30 vol% of the rock.

The plutonic rocks are granitic, mainly occupying the northwestern part of the study area. These granites both show mesocratic and leucocratic in composition. These intrusions are locally crosscut by diverse dolerite dykes measuring up to 2 m. The mesocratic granite samples strongly responded to the magnetic pen, while no response was recorded from the leucogranites and most of the aplite dykes in the area. Aplite dykes are abundant and mainly hosted by mesocratic granites (Fig. 3c). These mesocratic granites are the most abundant in the area. Generally, they occur as a medium to coarse-grains, locally porphyritic (Fig. 3a, c) containing quartz, k-feldspars, plagioclase, biotite, hornblende (Fig. 3d), and in some cases with epidote (Fig. 3a, b). The hornblende-epidote-bearing granites occur as medium-grained, considered to be rare granite in the Region. Both microcline and orthoclase are common in the mesocratic granites, displaying moderate to intense perthites structures. Epidote is commonly zoned in the hornblende-biotite-bearing granites. The microcline commonly bears inclusions of, quartz and accessory titanite. Zircon also forms part of the accessory group while the opaque minerals, sericite, chlorite, muscovite and epidote are secondary occupying mineral interstices.

The leucogranites vary from medium to coarse-grained, and occur as isolated plutons in the area. They bear vugs and cavities healed by quartz and locally crosscut by mafic dykes. Quartz is highly abundant in these granites occurring alongside plagioclase, and orthoclase, displaying granophyric structures (Fig. 3e, h). The ferromagnesian minerals occur mostly in clusters with single grains very uncommon. These minerals include: hornblende, arfvedsonite, clinopyroxene and aegirine (Fig. 3f, g). The accessory minerals include muscovite, tourmaline, cassiterite, titanite, zircon, opaque minerals alongside secondary quartz and sericite.

Volcanic rocks are essentially made up of rhyolite and locally outcrop in Nwe and Petit Atta areas as dykes extending over 50 m long and 20 m large. The structure of the dykes is polygonal with individual polygon varying from square to rectangular and measures from 20 to 30 cm large. Micro-texture of these rhyolites show phenocrysts of quartz and sanidine embedded within a fine-grained groundmass giving the rock a porphyritic aphanitic texture.

4.2 Geochemistry

Results from whole rock geochemical analysis show that these rocks are general high potassic rocks. However, the paragneisses (Garnet-Sillimanite gneiss) (Fig. 2e, f) show mean SiO_2 content of 68.3 wt.%, Al_2O_3 = 14.33 wt.%, Fe_2O_3(T) = 6.67 wt.% and MgO = 2.23 wt.% that correlate negatively with SiO_2. CaO, Na_2O and K_2O vary respectively as 2.0 wt.%, 2.27 wt.% and 1.91 wt.%. The

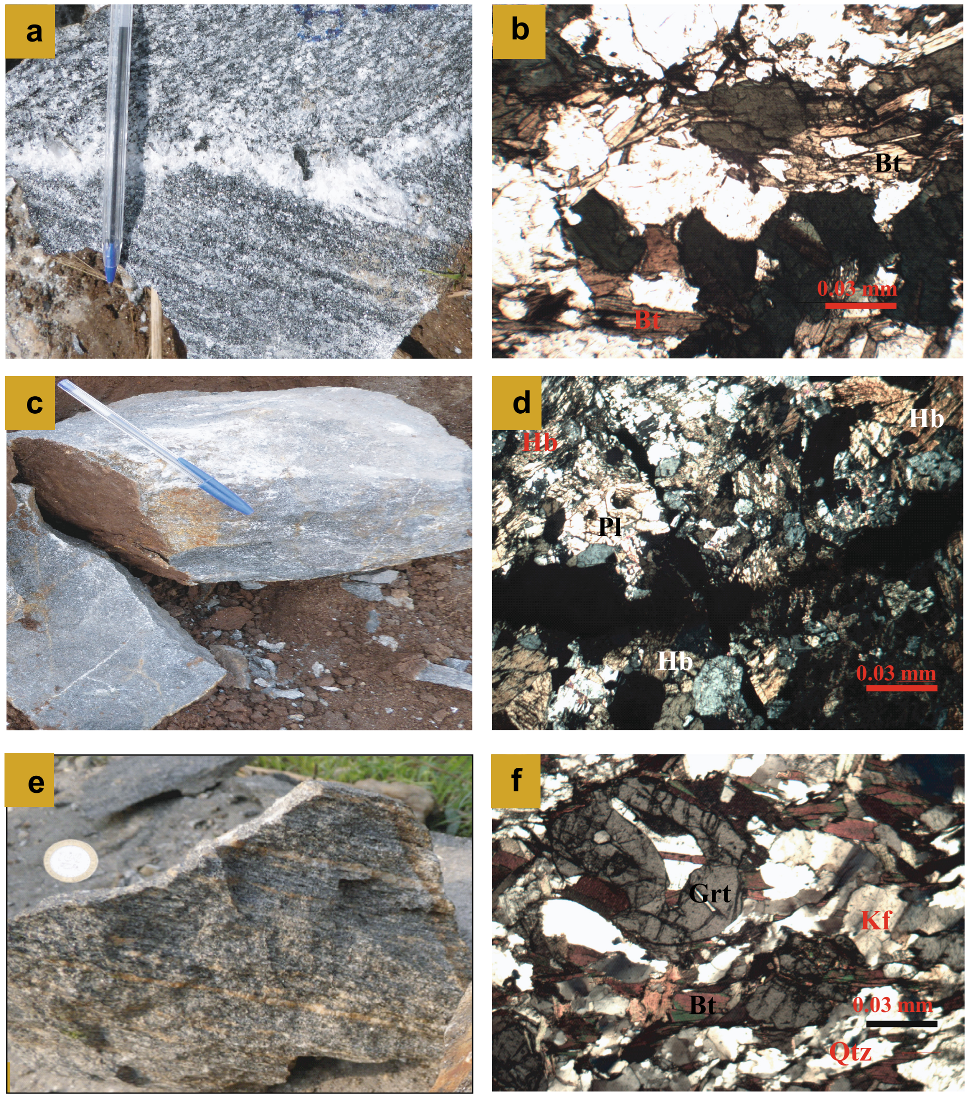

Fig. 2 Rock samples and photomicrographs of gneisses. **a**, **b** orthogneiss; **c**, **d** hornblende-bearing gneiss; **e**, **f** paragneiss; *Bt* Biotite, *Hb* Hornblende, *Kf* k-feldspar, *Qtz* Quartz, *Grt* Garnet, *Pl* Plagioclase. Mineral symbols after Kretz (1983); Whitney and Evans (2010)

mean TiO_2 content is 0.87 wt.%, while P_2O_5 has mean values less than 1 wt.%. The trace elements show moderate Ba (869 ppm), Rb (61 to 92 ppm), Sr (222 to 312 ppm) and low Nb (3–11 ppm), Zr (199 ppm), Hf (5.1 ppm).

In this area, the orthogneisses (Fig. 2a, b) show similarity in their major element composition to the mesocratic granites. However, they differ in their tholeiitic to calc-alkaline nature (Fig. 4a). These gneisses (Biotite-bearing, Hornblende-Biotite-bearing, Hornblende-bearing gneisses) are high in SiO_2 and range from 50.1 to 74.13 wt.%, while Al_2O_3 content range from 14.45 to 18.6 wt.%. The Fe_2O_3 (T) content is higher than MgO ranging from 1.16 to 11.09 wt.% and 0.09 to 4.8 wt.% respectively. MnO vary from 0.02 to 0.63 wt.%, TiO_2 from 0.49 to 0.86 wt.% and P_2O_5 from 0.12 to 0.19 wt.%. CaO, Na_2O and K_2O are moderate with values ranging from 0.77 to 4.43 wt.%, 4.38 to 4.48 wt.%, and 1.71 to 2.73 wt.% respectively. The highest Fe_2O_3(T) and CaO contents are observed in the Hornblende-bearing gneisses and amphibolites with Fe_2O_3(T) and CaO varying from 6.96–11.09 wt.% and 7.67–17.23 wt.% respectively. The mol proportion Al_2O_3/$CaO + Na_2O + K_2O$ (A/CNK) of these gneisses vary from 0.38 to 1.04 (Fig. 4b) with $K_2O + Na_2O$ (KN) ranging from 0.93 to 7.11 wt.%. The trace elements content show enrichment in Large Ionic Lithophile Elements (LILE) such as Ba (149 to 2315 ppm), moderate Rb (8 to 225 ppm) and Sr (112 to 1100 ppm) while the High Field Strength Elements (HFSE) show depletion in Nb (2 to 12 ppm), Zr (114 to 256 ppm), Hf (1.4 to 6.6 ppm) and Ta (0.2 to 2.8 ppm). However, their mineralogical similarity to the mesocratic granites is consistent, with depletion in Nb, Ti, P and enrichment in Pb and Dy. The ratios of Rb/Sr vary from 0.1 to 29.73, Rb/Sr from 0.1 to 0.56, Sr/Y from 11.2 to 91.67 and K/Rb from 21.33 to 2537. The Eu content shows no pronounced negative anomaly with the ratio of $(Eu/Eu^*)_N$ ranging from 0.29 to 1.27. LREE also shows

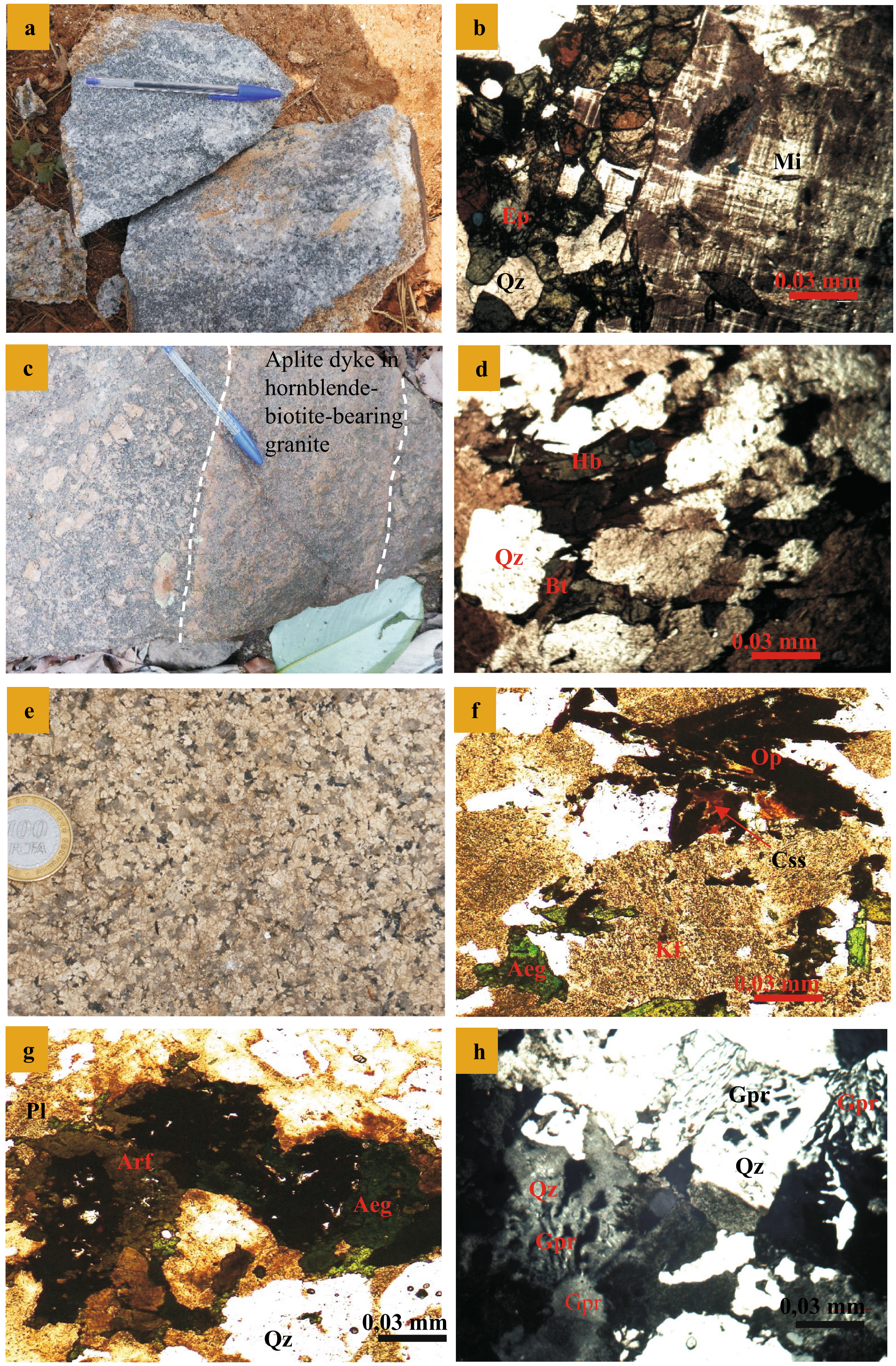

Fig. 3 Rock samples and photomicrograph of granites; **a**, **b** mesocratic hornblende-epidote-bearing granite; **c**, **d** porphyritic hornblende-biotite-bearing mesocratic granite; **e–h** course-grained amphibole-pyroxene-bearing leucogranite; rhyolites, *Qtz* Quartz, *Mi* Microcline, *Pl* Plagioclase, *Aeg* Aegirine, *Arf* Arfvedsonite, *Css* Cassiterite, *Op* Opaque, *Bt* Biotite, *Sn* Sanidine, *Gpr* granophir, *Gm* Groundmass. Mineral symbols after Kretz (1983), Whitney and Evans (2010)

enrichment relative to the HREE with the ratios of $(La/Lu)_N$ varying between 2.29 to 30.01, $(La/Yb)_N$ between 2.29 to 29.73 and $(Dy/Yb)_N$ between 0.94 to 1.95.

Geochemical results for mesocratic granites (Biotite-bearing, Hornblende-Biotite-bearing and Hornblende-Epidote-bearing granites) show that they are generally shoshonitic (Fig. 4a). They show high SiO_2 contents ranging from 65.33 to 72.87 wt.% with an average of 70.19 wt.%. Al_2O_3 content is high, with values from 13.35 to 15.48 wt.% (mean of 14.92 wt.%). Fe_2O_3(T) is slightly higher than MgO varying from 0.56 to 3.98 wt.%, 0.03 to 1.54 wt.% with means of 2.42 wt.% and 0.79 wt.% respectively. Na_2O and K_2O content are equally low and range from 3.25 to 4.18 and 4.66 to 6.45 wt.% with means of 3.46

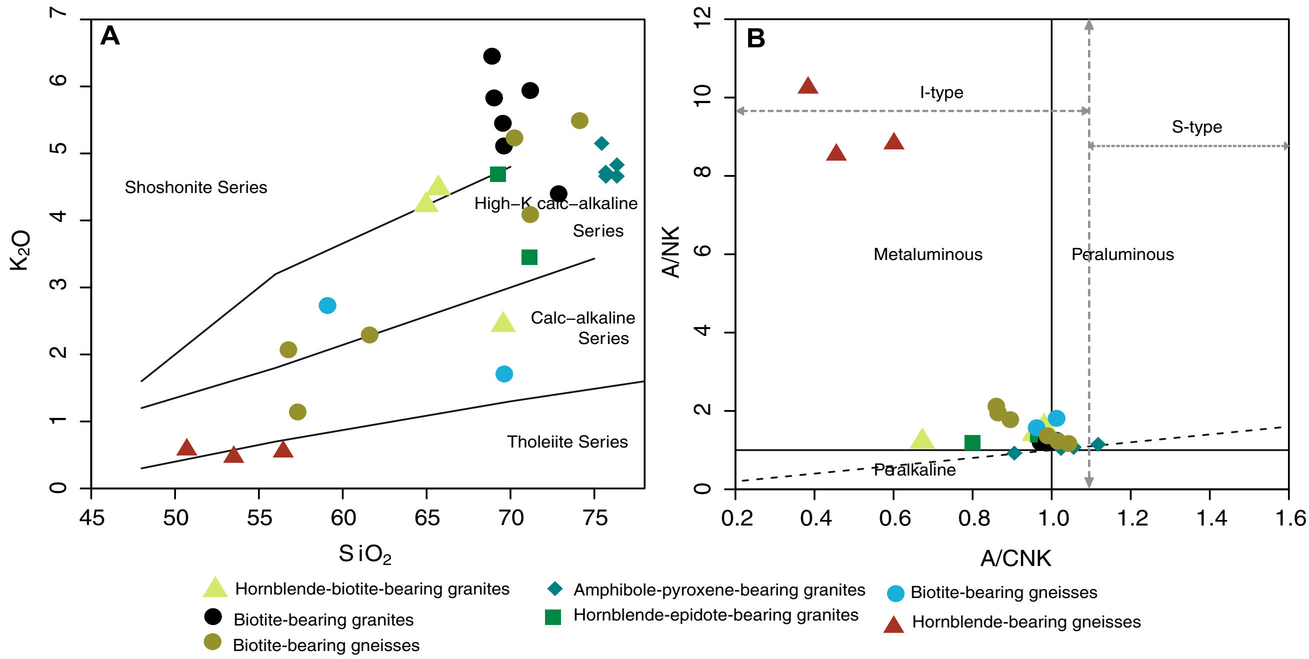

Fig. 4 K_2O versus SiO_2 (Peccerillo and Taylor 1976); and A/NK versus A/CNK (Frost et al. 2001) diagrams showing the composition of Somie-Ntem granitoids. I and S-type boundary adopted from Chappell and White (1992)

wt.% and 5.53 wt.% respectively. Meanwhile, the CaO content is relatively lower compared to K_2O and Na_2O and varies from 0.06 to 4.14 wt.%. These granites show metaluminous I-type affinity with the molar proportion of A/CNK ranging from 0.64 to 1.04 (Fig. 4b). MnO is very low with about 0.04 wt.% on average while TiO_2 has a mean content of 0.46 wt.% and P_2O_5 mean of 0.15 wt.%. The trace elements content for these granites shows very high Ba (677 to 2592 ppm), Rb (96 to 224 ppm), Sr (563 to 834 ppm) and Zr (161 to 428 ppm). In general, the LILE are enriched relative to the HFSE such as Hf (0.4–10.6 ppm), Nb (6–13 ppm), Ta (0.8–5.8 ppm) and Zr (14–428 ppm). These granites also show depletion in Nb, Ti, P, while Pb is strongly enriched. The trace elements ratios vary considerably, with Rb/Sr ranging from 0.16 to 0.4, Ba/Rb from 7.39 to 12.58. Similarly, the LREE shows high fractionation relative to the HREE as indicated by the ratios of $(La/Yb)_N$ ranging from 10.67 to 69.95, $(La/Sm)_N$ from 3.38 to 8.43 and $(Dy/Yb)_N$ from 0.98 to 1.73. The Eu shows moderate negative to a slightly positive anomaly with $(Eu/Eu^*)_N$ = 0.52 to 1.05.

The leucogranites (Amphibole-Pyroxene-bearing granites) show high-K calc-alkaline affinity (Fig. 4a). They contain very high SiO_2 ranging from 75.44 to 76.39 wt.%, Al_2O_3 from 11.26 to 12.90 wt.% while Na_2O and K_2O contents range from 3.37 to 4.36 wt.% and 4.66 to 5.15 wt.% respectively. A/CNK values range from 0.9 to 1.14 thereby placing them in the peraluminous I-type to slightly S-type fields (Fig. 4b). The total alkali content is high with $K_2O + Na_2O$ (NK) varying from 8.09 to 9.02 wt.%. $Fe_2O_3(T)$ content is moderate relative to MgO, with a mean value of 1.95 wt.% and 0.02 wt.%, respectively. Mean P_2O_5 is 0.03 wt.%, while TiO_2 and CaO are very low, with means of 0.03 wt.% and 0.17 wt.%, respectively.

In terms of their trace element content, the leucogranites show LILE very low in Ba (15–79 ppm) Sr (4–9 ppm) and high in Rb (153–261 ppm). Whereas, the HFSEs show enrichment in Nb (37–76 ppm), Zr (558–1261 ppm), Hf (5.7–20.4 ppm) and Ta (4–7.6 ppm). A pronounced negative Eu- anomaly is observed, with $(Eu/Eu^*)_N$ varying from 0.08–0.14. Also, ratios of Rb/Sr range from 17.22 to 65.25, K/Rb from 163.6 to 252.94, Nb/Ta from 7–9.66, Zr/Hf from 20.35–44.41, Sm/Eu from 6.86–16.68 and Sr/Y from 0.03 to 0.14 except for one sample (B120-2) with a high Sr/Y ratio of 346. LREE are relatively high compared to the HREE with $(La/Lu)_N$ = 3.66–49.10, $(La/Yb)_N$ = 3.66–14.43 and $(Dy/Yb)_N$ = 0.8–1.77.

5 Discussion

5.1 Mineral potential evaluation

Selected ore elements from the data have been tested for normal distribution using histograms and box plots. Histogram representations (Fig. 5) generally show skewness in the distribution of ore elements within the rocks. The selected ore elements in the analyzed samples are all skewed to the right. Elements with anomaly high concentrations occur as isolated bars to the right. This indicates that the concentration of elements in the latest bars falls above the upper threshold. Histogram bars further to the left are samples with the maximum concentration of the respective trace metal closer or above the upper threshold, thus constitute the positive anomalies in the sample population. However, most element distribution show multiple populations indicated by the separation of the histogram bars (two population concentrations), which is common with geochemical data distribution (Reimann and Filzmoser 2000; Reimann et al. 2005). The difference in the distribution of the elements in the rocks suggests variation in composition due to; magmatic contamination, fractional crystallization and post-magmatic alteration of the parent magma (Reimann and Filzmoser 2000).

Box plots representations for the selected trace metals show an overall downwards skewness. At the same time, the outliers are found on the upper side of the box. This is an indicating that the concentration of the respective trace metals in the rocks are low and clusters around the lower percentile (Fig. 6). Meanwhile, the calculated threshold for the element concentrations in the samples shows anomalies in some samples. In general, the elements Al, Ag, Cr, Cu, Cs, Hf, Nb, Ni, Sc, Sn, Ta, Th, Ti, U, V, Y and Zn show enrichment. However, three groups of mineralization have been interpreted here in relation to the rocks type (Table 1). Leucogranites show potential for Sn-Zn mineralization and occur in association with Hf, Nb, Ta, and Y, while mesocratic granites are generally poor in these elements but host an aplite dyke that show strong enrichment for U and Th (Fig. 7). The metamorphic rocks are slightly enriched in Al, Ag, Mg, Mn, and Ti. However, the mafic hornblende-bearing gneisses of this group show strong potential for Cr–Cu–Ni–V mineralization. The enrichment in Cr is also observed in the amphibolites (Table 1).

5.2 Sn-Zn mineralization

Sn-Zn mineralization in this area occurs within the leucogranites that display a high-K calc-alkaline nature with peraluminous I to slightly S-type affinity (Fig. 4a, b). These are the youngest intrusions in the area with post-orogenic setting, emplaced in a within plate environment (Fig. 8b, c). The within plate environment is typical for skarn-type Sn- mineralization (Meinert 1995); However, this may vary depending on the type of magma. According to Sillitoe (1996), I-type magmas concentrate more Fe, Cu, Mo and Au while S-types are best for Sn and W (Govett and Atherde 1988; Ghodsi et al. 2016). Meanwhile, Bues (1968) believes that every granite has potential for a particular mineralization type, which could either be magmatic or hydrothermal. The Sn–Zn-bearing granites show high SiO_2, Nb, Hf, Ta, and Zr contents common with such mineralized granites (Kovalenko 1978; Tischendorf 1977; El Gharbawy and Maadawy 2012). McCarthy and Hasty (1976) established a good positive relationship between Ba, Rb, Sr and Sn mineralization. According to Groves and McCarthy (1978), depleted Ba and Sr in granitic rocks correlate well with Sn mineralization. This relationship has been observed and demonstrated in the discrimination diagram of Blevin (2003) on barren and fertile rocks (Fig. 9a–d) using K/Rb versus SiO_2, and also SiO_2 versus Fe_2O_3(T), Zn versus SiO_2 (Wolfe 1977) and Rb–Ba–Sr (Karimpour et al. 1983). Based on the representations, the leucogranites are the most fertile and plot perfectly within the field of Sn-bearing granites (Fig. 9c). The trace elements characteristics show that these granites were enriched through high post magmatic metasomatic based on several factors. The first observation is in their high Zr/Hf > 20 and K/Rb > 100, which is common with rocks affected by moderate to week hydrothermal activity (Cerny and Burt 1984; Bea et al. 2006; Rossi et al. 2011). In other words, hydrothermal activity was not intense to influence Sn-Zn mineralization in the granites. Usually, hydrothermal processes such as sericitization and silicification cause the loss of Sr and Rb within the feldspars but these granites show no depletion in Rb. Imoekparia (1981) also demonstrated the relationship between Sn-bearing granites and Rb ratios whereby high Rb/Sr and low Ba/Rb ratios were observed with Sn-bearing granites, especially the younger post orogenic granites as is the case with the Somie-Ntem leucogranites showing high Rb/Sr (1.22–65.25) and low Ba/Rb (0.06–0.51). With several debates put forward regarding the origin of Sn mineralization in granites, most models propose intense post-magmatic metasomatism involving albitization and topazization (Beus et al. 1962; Stemprok 1971; Haapala 1997). Others propose specialized granites derived from post-magmatic modification of the original rock by hydrothermal fluids (Haapala 1977, 1995). From Haapala (1997), the magmatic source for Sn-bearing granites contains topaz-bearing fluid inclusions due to late-stage crystallization.

Though topaz is not evident in the Somie-Ntem granites, they display some petrographic and geochemical characteristics common with most Sn-bearing granites, such as the presence of granophyric structures and mairolitic cavities (Haapala 1997); the association of tourmaline, cassiterite, muscovite with abundant quartz (Wang et al. 2017), low Ba, Sr, Ce, Ti, Eu, high Rb, Th, U, Nb, Zr, Ga (Ti-Schendorf 1977; Haapala 1997) and high Rb/Sr, K/Rb, K/Ba (Imoekparia 1981; Horbe et al. 1991; Ogunleye et al. 2005). Though some of these characteristics do not quite

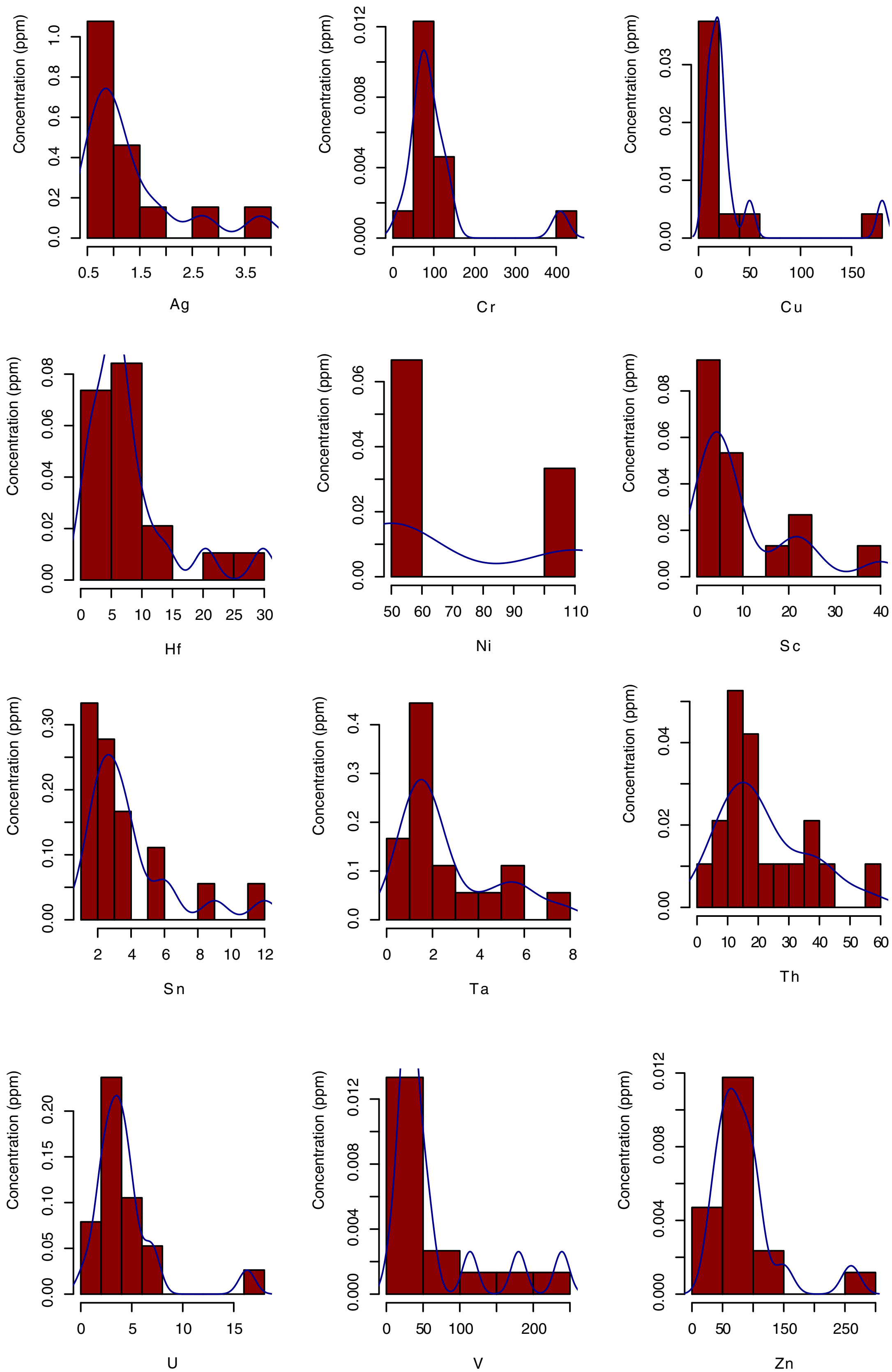

Fig. 5 Histograms showing the distribution of ore elements within rocks of the study area

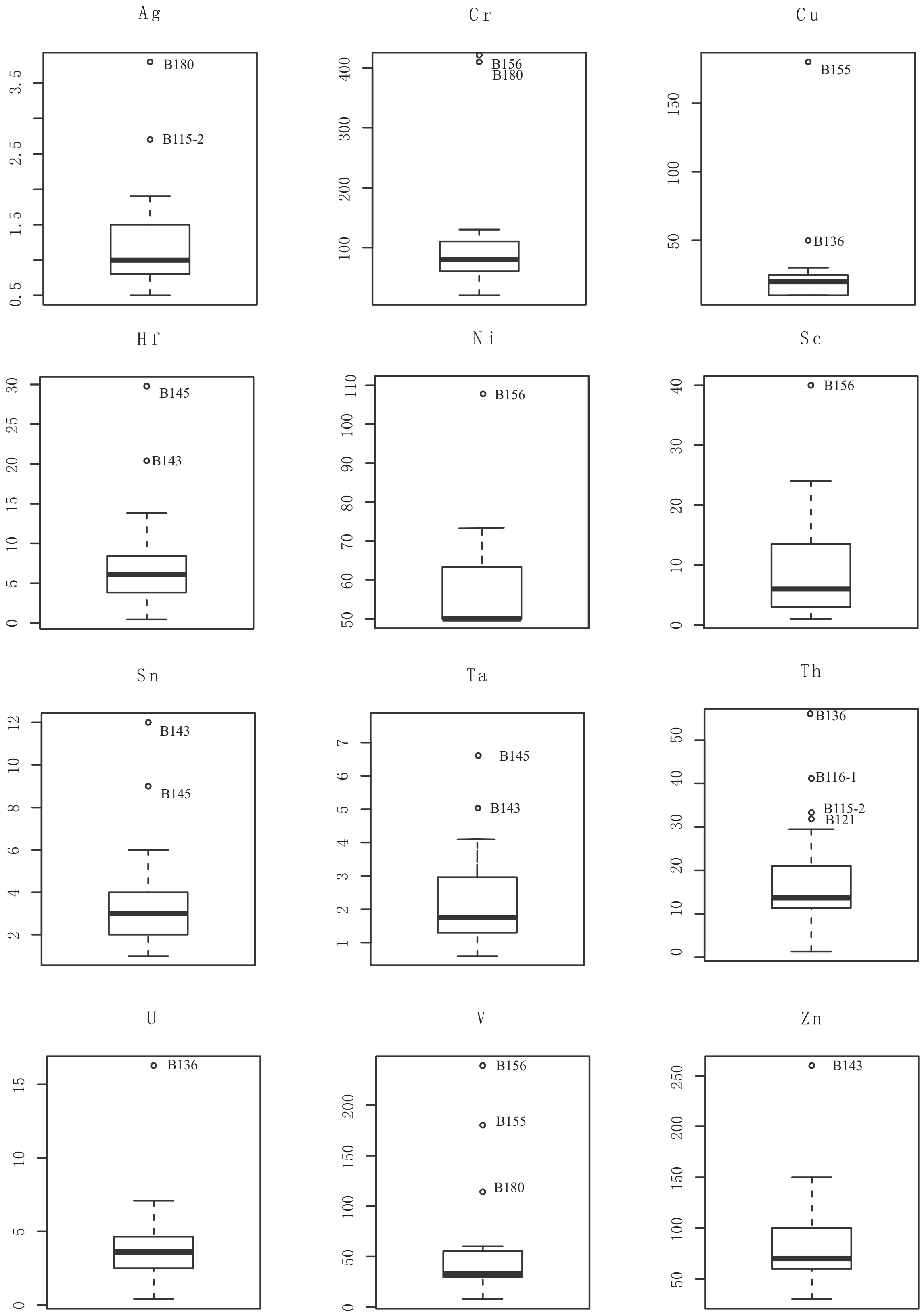

Fig. 6 Box plots showing the variation in the concentration of trace metals in the rock samples with anomalies as outliers

Table 1 Statistical trace elements concentration (ppm) in rocks of study area (Wedepohl 1995)

Elements	Rock type enriched	No of samples	Enriched sample	Mean	Min	25%	50%	75%	Max	Calculated threshold	Crustal abondance
Cr	Hornblende-bearing gneiss/amphibolite	20	B156 B180	116	20	60	85	115	410	198	200
Cu	Hornblende-bearing gneiss	18	B155	31	10	12	20	27	180	50	68
Ni	Hornblende-bearing gneiss	5	B156	62	40	50	50	60	110	75	80
Sn	Leucogranite	29	B143 B143	3.5	1	2	3	4	12	9	2
Th	Aplite dyke (mesocratic)	30	B115-2 B136	17.2	1	9.2	14	20	55.1	36.2	8–18
U	Aplite dyke (mesocratic)	30	B115-2 B136	4	0.3	2	3	5	16.3	10	3–3.5
V	Hornblende-bearing gneiss	24	B156	69.6	8	30	48	98	239	200	150
Zn	Leucogranite	27	B143 B145	86	30	60	80	100	260	160	65

justify a magmatic origin, the presence of muscovite and the rare cassiterite show a strong connection to a magmatic source (Gomes and Neiva 2002).

Information on post magmatic mineralization would require an alkali-volatile phase during crystallization for Sn to form (Olade 1980). The depletion in MgO, CaO, TiO_2 together with Ba and Sr in these granites rather suggest high fractionation process with the removal of Mg-rich olivine, calcic pyroxene, amphibole, feldspars and FeTi oxides (Girei et al. 2019). However, the trace element signatures show a connection with Cl-rich systems for this mineralization. Based on previous reports, the concentration of elements like Rb, Cs, U, Th and HREE in a silicate melt is related to Fe-rich systems unlike Cl-rich systems that turn to concentrate Zr, Hf, Ta, Y and LREE (Taylor et al. 1981). Meanwhile, these granites show compositional similarities to Sn-bearing granites elsewhere around the world (Ekwere 1985; Imeokparia 1981, 1985, 1990; Horbe et al. 1991). For example, correlation in Rb/Sr, Sm/Eu, Zr/Hf, K/Ba, Ba/Rb, Nb/Ta, Th/U and $(La/Yb)_N$ ratios (Table 2, Fig. 10) with those of younger Sn-granites of northern Nigeria (Ogunleye et al. 2005). The similarity in these ratios supports the involvement of volatile fluids during postmagmatic alteration. It is quite common that Sn-bearing granites show enrichment in Sn, Nb, Ta, Zr, Y, HREE and Li (Imeokparia 1983; Kinnaird 1985; Harris et al. 1986; Horbe et al. 1991; Ogunleye et al. 2005) similar to the ones in the study area. Even with the presence of aegirine, arfvedsonite, titanite and quartz coupled with the absence of biotite in these Sn-bearing granites, (Bahajroy and Taki 2014; Goswani et al. 2015), the association of these elements indicates that volatile fluids were involved for their complexation and transport to the roof within the magmatic system (Whalen et al. 1987; Imeokparia 1993; Horbe et al. 1991; Ogunleye et al. 2005). Aegirine presence also indicates a situation of increasing oxidation of the late magmatic fluid during melt crystallization, thereby favouring the dissolution of Na into the fluid (Marks et al. 2003). Arfvedsonite crystals occur in association with aegirine in these leucogranites suggesting a process of destabilization in crystallization temperature with increased oxidation that caused aegirine to be unstable in favor of arfvedsonite (Goswani et al. 2015).

Ogunleye et al. (2005) established a link between Sn-bearing granites and albitization. According to their findings, albitization in association with arfvedsonite gave the highest potential for Sn than the normal aegirine-arfvedsonite and arfvedsonite bearing granites. Notwithstanding, the Sn-bearing granites in the Somie-Ntem area show no signs of albitization due to the lack of Na_2O enrichment. This could mean that Sn is probably substituted in the mineral structures of pyrochlore and Nb-rich accessory phases alongside individual mineral phases like cassiterite (Ogunleye et al. 2005).

Though the presence of cassiterite signifies magmatic origin for Sn, the occurrence of tourmaline, a dense network of granophyric structures (Barker 1970; Cox et al. 1979), strongly advocate for post magmatic/eutectic crystallization during the evolution of the granites. According to Shelley (1966), granophyric texture with feldspar phenocrysts surrounded by groundmass as in these leucogranites signifies melt crystallization with simultaneous reaction and partial melting of the country-rock while undergoing slow cooling. Thus, the granophyric

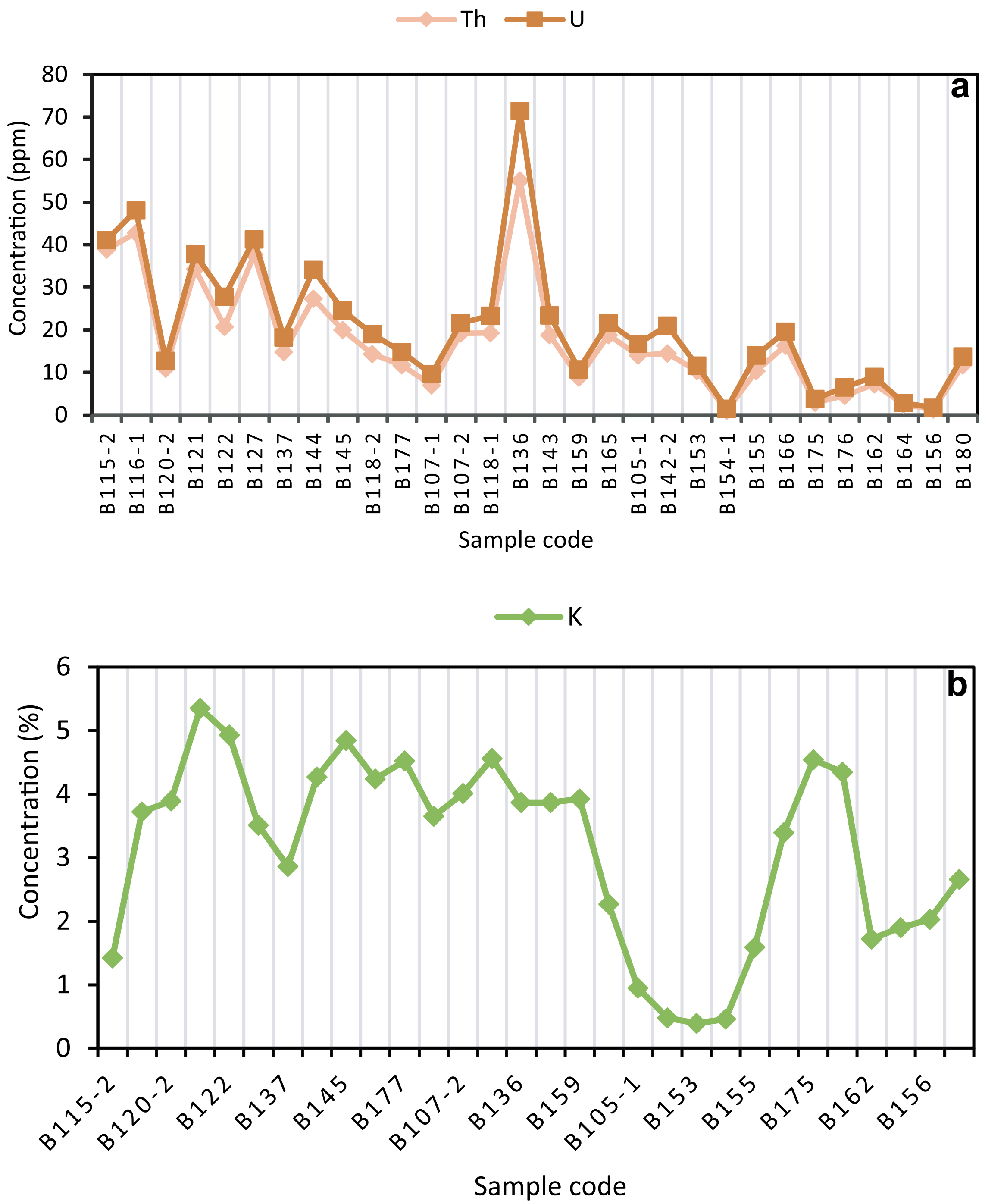

Fig. 7 Spider plots showing variation in K, Th and U from whole-rock geochemistry in samples from the Somie-Ntem area

leucogranites of this area might have formed under different pressure and water conditions with a simultaneous crystallization of quartz and k-feldspars from a viscous granitic melt cooling below its liquidus temperature (Strauss 1954; Morgan and London 2012). However, a proposed model for Sn-mineralization in such granites has also been explained in Groves and McCarthy (1978), which says the crystallization of such magma commence from the roof and floor of the chamber, then progresses inwards with a progressive fractionation till the point of water saturation whereby the Sn-poor vapour becomes separated and collect to form barren structures while the water-saturated melt enriched in Sn, F and/or B further crystallizes causing greisenization. Thus greisenization (Stemprok 1987), silicification and tourmalinization (Strauss 1954) could be responsible for the high SiO_2 (75.68–76.35 wt.%) content

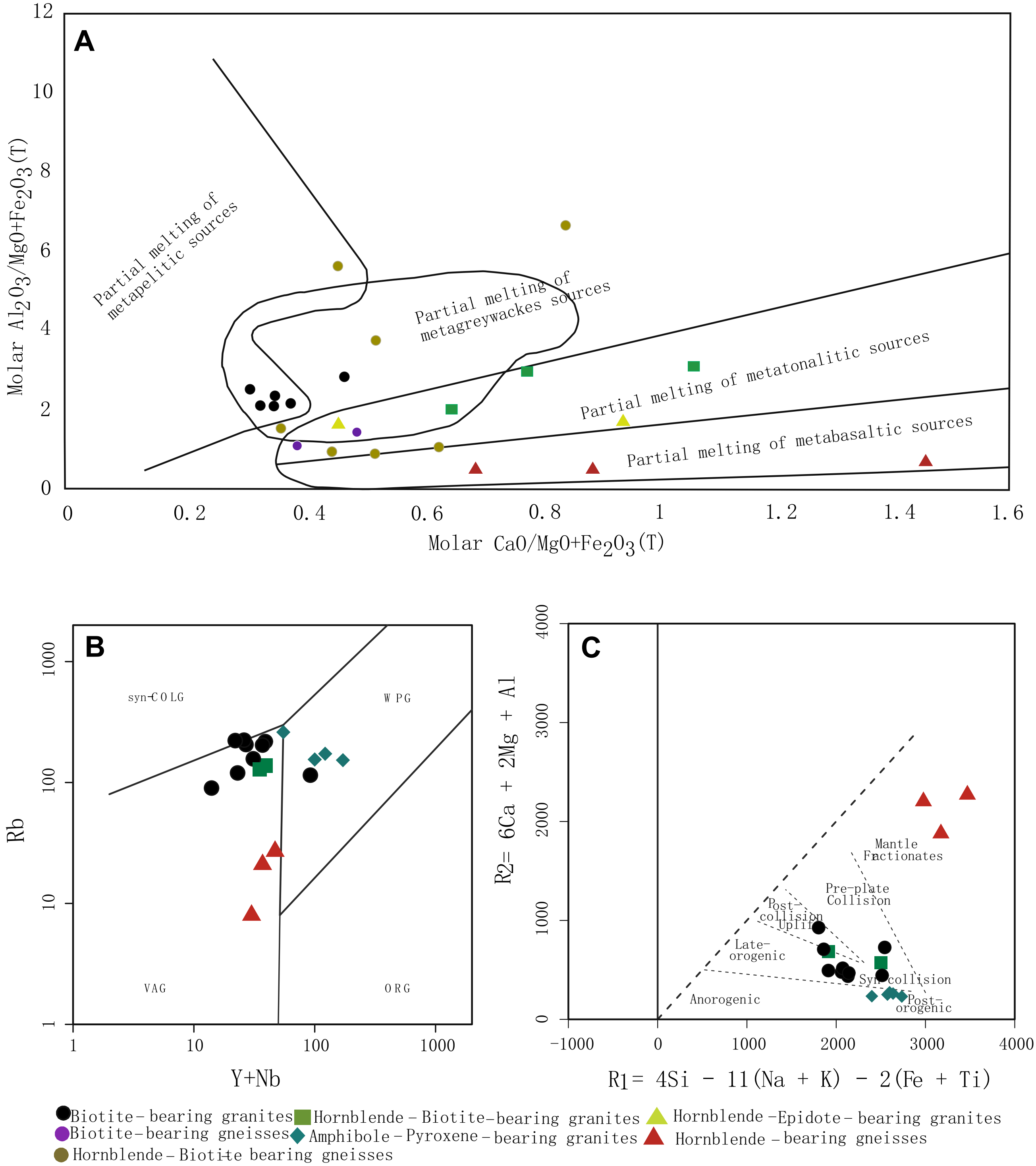

Fig. 8 Discrimination diagrams showing tectonic setting for granitic rocks in the study area. **A** Molar diagram of CaO/(MgO + FeOt) versus Al_2O_3/(MgO + FeOt) (Gerdes et al. 2002); **B** Y + Nb versus Rb of Pearce et al. (1984); **C** R_1–R_2 millications diagram of Batchelor and Bowden (1985)

in the Somie-Ntem Sn-bearing granites during which quartz, muscovite, tourmaline, and cassiterite (importing Sn, Rb) were remobilization at the expense of biotite and feldspars decomposition in the semi-solidified state.

In general, the release of metallic elements is facilitated by dissolution reactions and solid–fluid exchanges in acidic, reducing and/or oxidizing chloride media, and by solid–fluid exchanges in neutral and oxidizing chloride

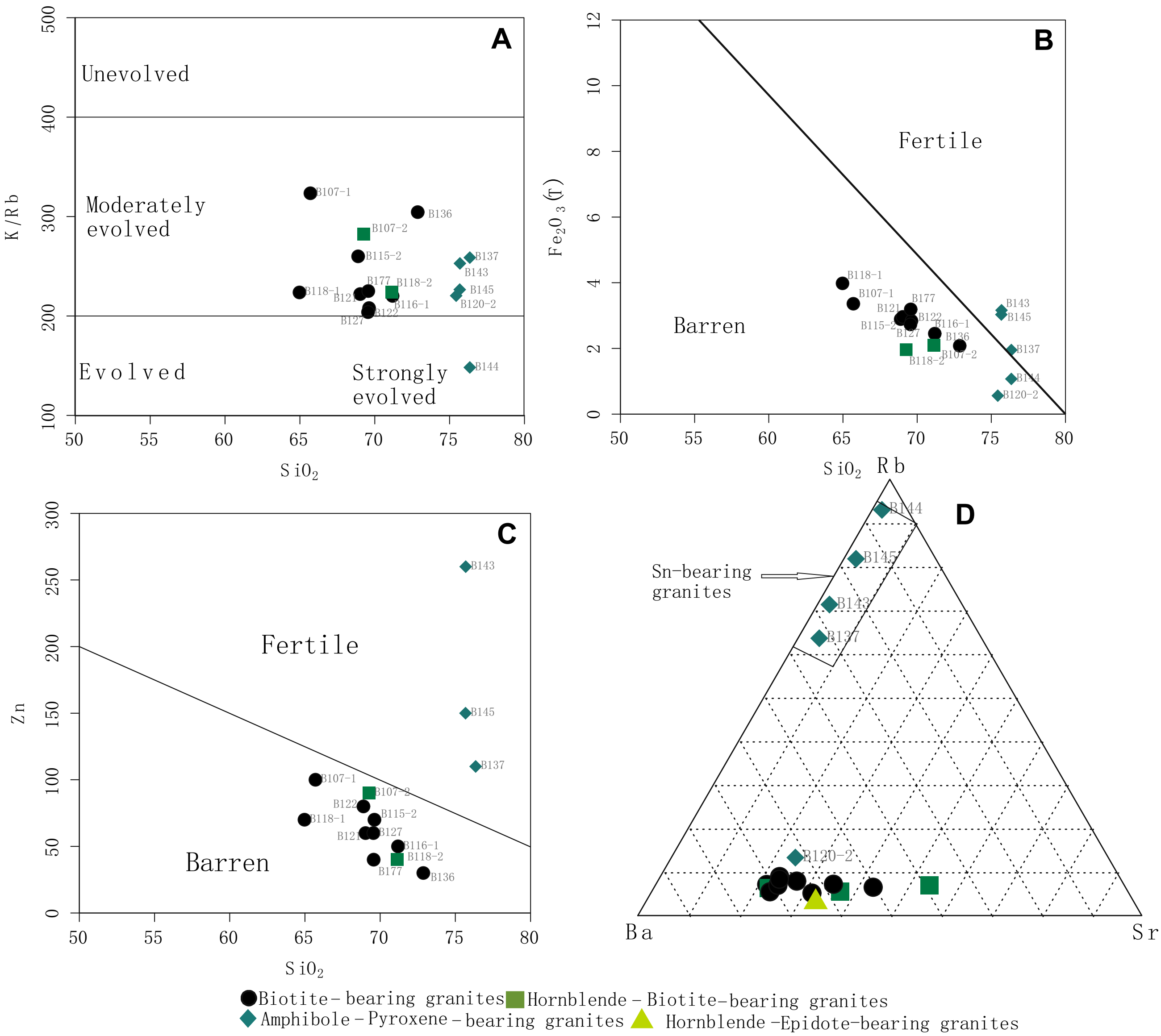

Fig. 9 Discrimination diagrams for fertile and barren granites within the Somie-Ntem area; **A** K/Rb versus SiO_2 (wt.%) after Blevin (2003); **B**, **C** Fe_2O_3(T) versus SiO_2; Zn versus SiO_2 (Wolfe 1977); **D** Rb–Ba–Sr (Karimpour et al. 1983)

media. The deposition of metal ores is the consequence of neutralization reactions. Metal chloride solutes precipitate as oxides and/or sulphides. In silicate rocks, neutralization is aided by the destabilization of alkali feldspars and biotite to muscovite and the production of brines (Bonin 1990). Hydrothermal processes consist of the remobilization of chemical constituents by hot aqueous fluids and are the consequence of the emplacement of magmas at a certain level of the crust. Of course, the nature of a magma varies according to the site where it is produced and emplaced (Chappell et al. 1998). This work is far from addressing the different aspects of the emplacement of a granitic massif with the interferences with their various enclosing rocks (example of greisenization of leucogranites or skarns).

5.3 U-Th mineralization

U-Th mineralization occur within an aplites dyke (Sample B136) hosted by mesocratic granites (Figs. 3a, b, 7a, b) that were emplaced in and arc/syn-collisional setting (Fig. 8b, c). Such mineralization is often considered intra-intrusive vein-type deposits (Banas and Mochnacka 1986, 1989; McKechnie et al. 2012, 2013). In some areas, their origins are attributed to metasomatism that caused the precipitation of REE, Zr, Th U, P and Nb (Gajda 1960a, b; Kanasiewicz

Table 2 Similarities in trace elements ratios between younger granites bearing aegirine and arfvedsonite in north western Cameroon (this study) and northern Nigeria (Nigeria values from Ogunleye et al. 2005)

Chemical characteristic	Cameroon Younger leucogranites	Nigeria Younger granites
Zr/Hf	44.41	25.26
Rb/Sr	38.25	36.99
Pb/Zn	0.07	0.20
Nb/Ta	0.37	8.32
Ba/Rb	9.66	0.40
Th/U	4.09	2.58
$(La/Yb)_N$	14.43	3.23
Zr/Nb	16.18	4.28
K/Rb	252.95	169.93
K/Ba	678.95	421.97

1988). The aplite dykes in this area show Th/U ratio of $\leq$ 3, 38 lower than the host mesocratic granites and fall in the same range as the leucogranites (Th/U average of 4.2) in the area. Reports show that granitic rocks with U-Th mineralization commonly display low Th/U ratios (Saleh and Kamar 2018) due to the fractionation of Th alongside Zr in the liquid (Bea 1996). The similarity in Th/U ratio between the aplite dyke and the leucogranites suggest a common source and emplacement time different from the host rock, probably from the same melt that emplaced leucogranites in the area. This goes in line with reports on U-Th mineralization occurring in leucogranites (Ibrahim et al. 2001; Kyser 2014). Moreover, reports within the Tikar plain (Ntieche et al. 2017; Yannah 2020), show that the emplacement of leucogranites in the area followed crustal extension along NE-SW faults. This resulted to the opening of fractures and subsequent healing by postmagmatic fluids. Even though this mineralization might only be confined to local faults genetically related to the regional NE-SW shear zone in the region since most aplitic samples were poor in U-Th. However, the Somie-Ntem mineralized dyke show some similarity in composition to the host mesocratic granites indicating that during dyke emplacement, a reaction between the injected fluid and the host rock probably occurred causing assimilation and mixing of material leading to compositional transition (both textural and chemical). Based on reports, these transitions in composition commence from the wall towards the centre of the dyke (Novák et al. 1999; Dini et al. 2004; Novák 2007) as field observation presents for the Somie-Ntem dykes showing chilled margins and the concentration of ferromagnesian minerals closer to the wall than at the center. However, further analysis is required to confirm to this effect. According to McKeough et al. (2013), the compositional gradient may cause enhanced diffusion of U, Th, Nb, Y and REE towards the rock-dyke margins, which may have to do with assimilation fractional crystallization leading to U-Th enrichment in some dyke-type mineralization (Shearer et al. 1992; McKeough et al. 2013). Melt fractionation is expressed in this dyke based on the decrease in the ratios of Nb/Ta with SiO_2 (Fig. 11a). The enrichment in biotite and titanite in the dyke might be responsible for the inverse relationship between $Fe_2O_3(T)$, CaO and MgO with SiO_2 in the rock samples (McKeough et al. 2013).

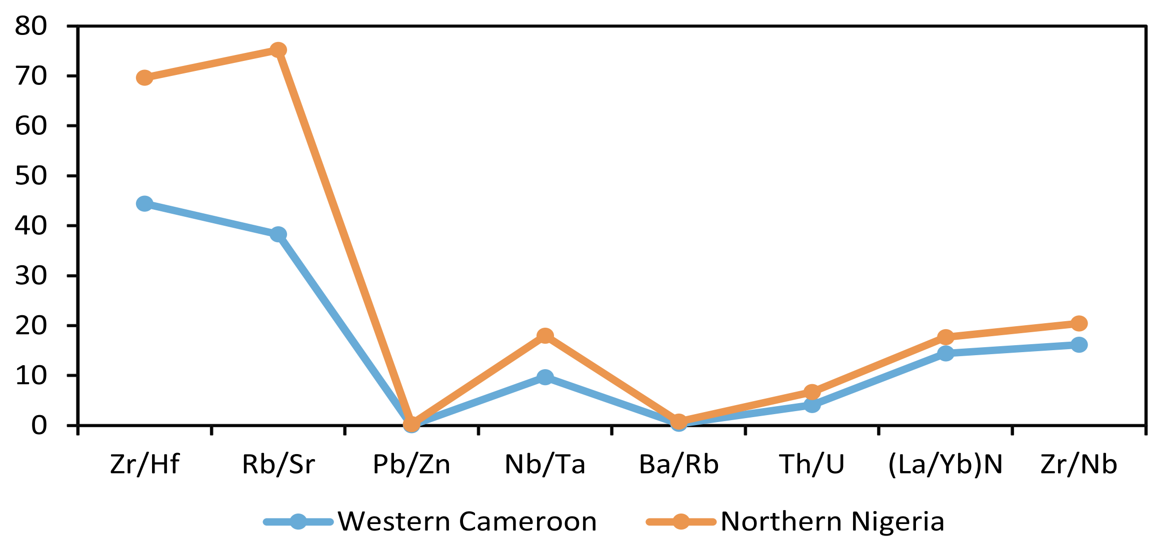

Fig. 10 Spider diagram showing similarities between aegirine-arfvedsonite granites from this work and Northern Nigeria (Nigeria data from Ogunleye et al. 2005)

Moreover, most mineralized aplite/pegmatite dykes are thought to undergo melt hybridization (Simmons and Heinrich 1980; Kretz et al. 1989; Owen 1989; Shearer et al. 1992; Lentz 1996). The varying ratios of Ba, Rb and Sr, the contrast in binary plots between Ta versus Nb/Ta, K/Cs versus U + Th and K/Rb versus Nb/Ta (Černý et al. 1986; Cerny 1971; Shearer et al. 1992; McKeough et al. 2013) generally indicate hybridization of the late melt during the emplacement of the dyke (sample B136) (Fig. 11b, d).

According to some authors (Pan 1997; Linnen 1998; Dostal and Chatterjee 2000; Linnen and Keppler 2002; McKeough et al. 2013), these trends signify crystal fractionation and subsequent injection of fluids. This is also supported by the high U, Th, Nb, Y and REE in the dyke which are strong indicators of hybrid fluids or silicate melt fluxes (London 2008; Simmons and Webber 2008; Nabelek et al. 2010; Van Lichtervelde et al. 2010; Linnen et al. 2012). The hybrid fluid may also be due to crustal contamination during their emplacement in a syn- to late tectonic regime (Fig. 8b, c). Even though Na-metasomatism and albitization have been reported for structural controlled U-mineralization in other areas within the WCD (Kouske et al. 2012), the lack of K trend for the dyke and host granites shows that albitization was irrelevant. Nevertheless, extreme fractionation or in situ partial melting of metasedimentary rocks may have influenced U-Th

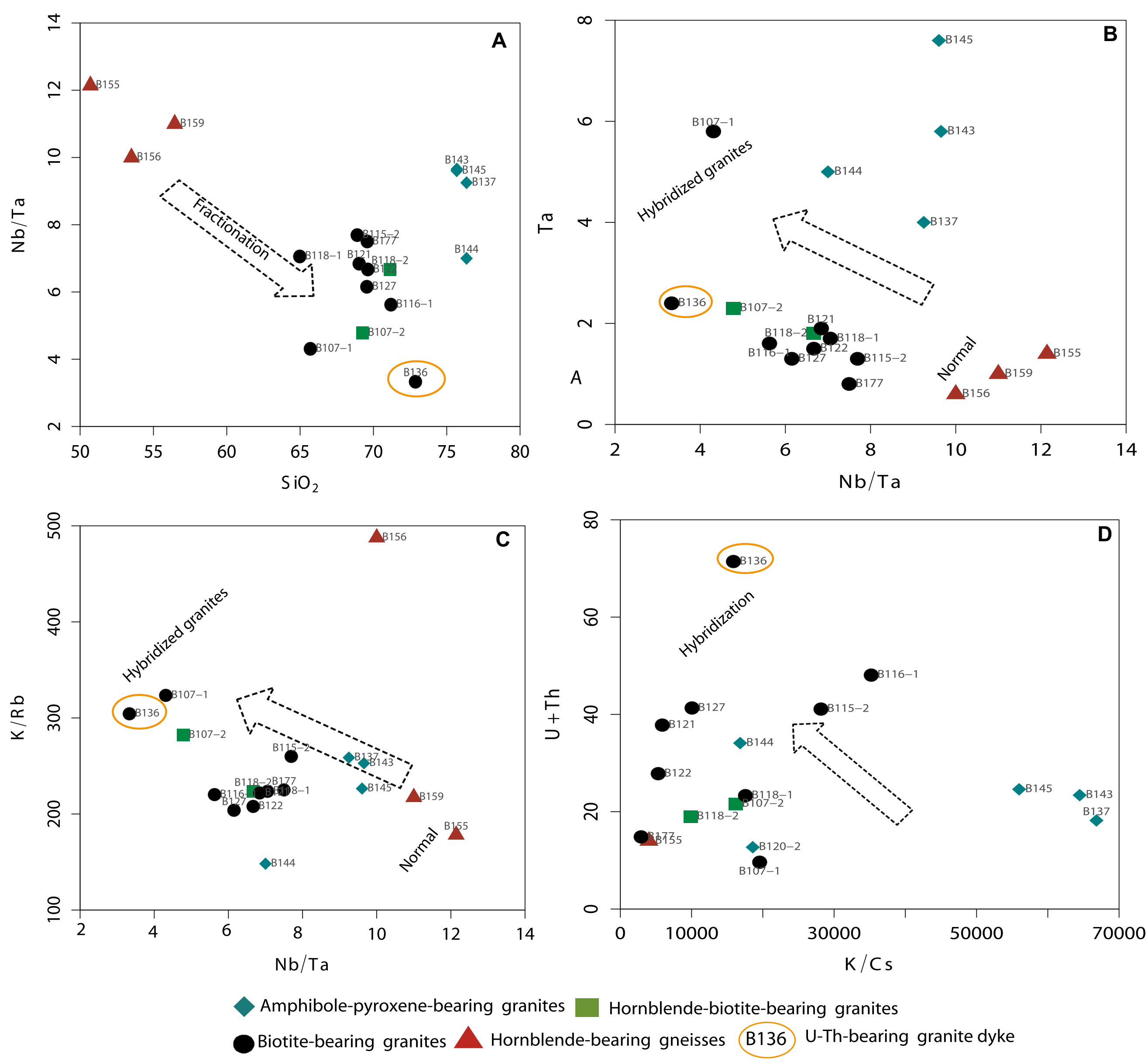

Fig. 11 Binary plots showing: evolution in granites in terms of melt hybridization: **a** melt grationation with variation in Nb/Ta versus SiO_2; **b–d** trend of hybridized melt (McKeough et al. 2013). Arrow indicates direction of increasing effect (e.g. sample B136)

enrichment in the dyke, not leaving out meteoric water influx that could enhanced leaching and mobilization of U in the rock.

5.4 Cr–Cu–Ni–V mineralization

This mineralization occurs in hornblende-bearing gneisses (orthogneisses) rich in plagioclase and green amphibole. As field and petrographic results indicate, the host rocks show features of brittle deformation with splays of fractures and veinlet healed by opaque minerals. The high concentration of their Fe_2O_3 content (10.8–11.1 wt.%) suggests hydrothermal magnetite alteration is involved although further analysis is required to verify this effect. Normally, hydrothermal activity is very unlikely to concentrate these trace metals considering their high compatibility with mantle rocks that deprive them of getting into the melt unless they were probably leached from mafic and ultramafic rocks along the conduit. In which case, this might indicate a possible Ni–Cu–PGEs deposit type in the area considering that the region forms part of the orogenic belt in central Africa. Previous studies show that magmatic terrains found in proximity to cratonic boundaries constitute suitable environments for Ni–Cu–PGEs-type mineralization (Naldrett 1999, 2009; Begg et al. 2010). Such terrains are often characterized by radial basic dykes such as the dolerite dykes identified in the Somie-Ntem area and the vicinity (Ntieche et al. 2016). Moreover, as indicated before, this area has a strong connection to the regional shear zone (CCSZ) that represents a major crustal discontinuity of the Pan-African orogeny (Toteu 1990; Ngako 1999) in the region. It forms the limit between Paleoproterozoic intracontinental domains (characterized by tonalite-trondhjemite-granodiorite formations) to the south (Nzenti et al. 1998; Makitie et al. 2019) and a juvenile active Paleoproterozoic to the north (Toteu 1990; Ngako 1999). These regional setting provide suitable environments for a lot of things to happen including transtensional and transpressional deformation, thrusting, accretion, magma intrusion (Archanjo and Bouchez 1991; Ngako et al. 2003; Toteu et al. 2004) and hydrothermal activities (Post 1999; Schulz et al. 2010). Thus, it is very likely to have sulfide mineralization and PGEs is such environments. Potential Cu–Ni–PGEs mineralization however, would require a primary mantle magma that was driven to high sulfide saturation before crystallization (Arndt et al. 2005). This is common in regions of crustal extension (Li et al. 2021) like the CAFB which might have caused rapids rising of mantle magma and emplacement of mafic bodies. In which case, the magma was subjected to several magmatic differentiation processes including fractional crystallization (FC) and crustal contamination (CC) of the rising partially melted lithospheric crust or mantle (Fig. 8a, c). Moreover, Cu and Co show no correlation with Zn as it should be for hydrothermal sulfide mineralization (Pelleter et al. 2016).

On the other hand, since sulfide fractionation into ultramafic rocks inhibits the transport of major base metals and sulfur (Li et al. 2021) to the surface, Cu–Cr–Ni–V mineralization might have involved stratabound hydrothermal activities (Hein et al. 2008) that was pen-contemporaneous to gneissification. But Ni show a strong positive correlation with V and Sc (Table 3) which goes to support the process of melt fractionation from a parent magma rather than post magmatic alteration as observed from the negative trends between Co V, and Sc with SiO_2 and positive with MgO (Fig. 12a–f). This is because melt fractionation will normally cause decrease in V, Ni and Sc as olivine and pyroxene get crystallized (Meinert 1995). Once the removal of olivine and pyroxene takes place, sulphur solubility and enrichment in FeO and silica content occur leading to sulfide segregation and mineralization (Lightfoot and Hawksworth 1997; Li et al. 2021; Barnes et al. 2016).

Other sources for Cu–Cr–Ni–V concentration in these rocks could involve melting of basaltic rocks due to the high Cu and Ni contents couple with the proximity of the study area to a major volcanic line (Cameroon Volcanic Line (CVL) in the region. But according to Fouquet et al. (2010), basaltic rocks do not contribute to Ni enrichment (Fouquet et al. 2010) in melts. Moreover, the Cu–Cr–Ni–V-bearing gneisses actually show mantle source emplaced in an arc (Fig. 8b, c) tectonic environment (Batchelor and Bowden 1985). This may have involved partial melting of mantle material at subduction probably with no significant metasomatic reaction considering that the rocks show low LILE, LREE, Ta and Nb (Zhao et al. 2016; Li et al. 2021). The rocks also display low to high Ni/Cu ratios that vary from 0.28 to 11. According to some reports, high Ni/Cu ratio is mostly associated with ultramafic rocks rather than basaltic which are generally low (Naldrett 1973; Schulz et al. 2010). The Ni/Cu ratio of 11 corresponds to either tholeiitic sill/dyke-type deposit or komatiitic Cu–Ni-type deposits around the world (Naldrett 2004; Naldrett et al. 2013). This means that the magmatic melt experienced high sulfur saturation early enough that the crystallization of olivine was not complete to absorb enough Ni from the melt (Mungall 2007). In that case, komatiite magma is very unlikely to form such mineralization due to their strong sulfide under saturation at crustal level unless their sulfide content was enriched through melting and assimilation of wall rock material (Lesher 1989). Other models propose for sulfide mineralization include (1) leaching of igneous rocks of variable compositions; and (2) sedimentary or seawater influx (Kuhn 2003; Hein et al. 2008; Hrouda et al. 2009; Gonzales et al. 2016). Overall, the concentration of Cr–Cu–

Table 3 Correlation between trace metals in hornblende-bearing gneisses within the study area

	Cu	Cr	Ni	V	Sc	Co	Zn
Cu	1						
Cr	− 0.65882	1					
Ni	− 0.37438	0.710554	1				
V	− 0.14523	0.597945	0.971734	1			
Sc	− 0.14523	0.597945	0.971734	1	1		
Co	0.646435	0.092649	− 0.04355	0.127417	0.127417	1	
Zn	− 0.07681	− 0.11032	− 0.77755	− 0.84273	− 0.84273	0.121506	1

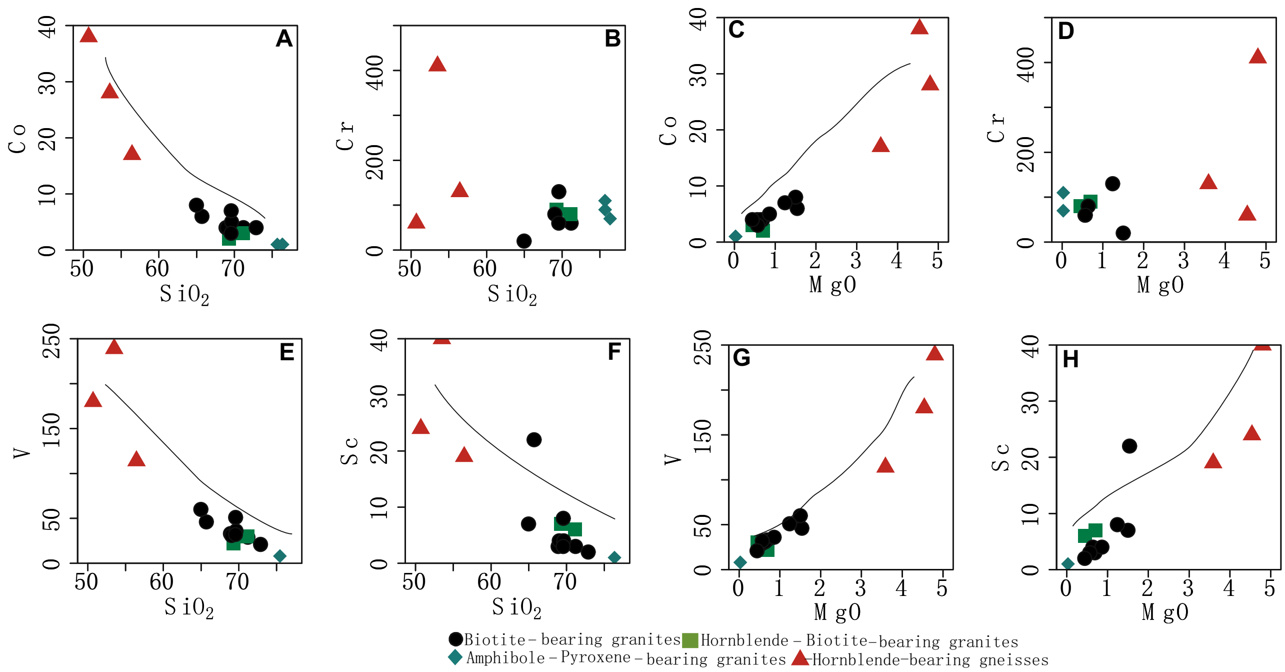

Fig. 12 Binary plots showing the evidence of fractional crystallization magmatic rocks bearing Cu-Cr-Ni-V mineralization

Ni–V mineralization in this area cannot be directly pinpoint to a particular process given the complex processes involved with magmatic evolution. The low Pb, depleted Mo and the lack of correlation between Co, Cu with Zn for hydrothermal input, the lack of calcite in the mineral assemblage of the rocks, the relationship with the regional geology, and the presence of mafic bodies within and around the study area, couple with the high Ni/Cu and very low Rb/Sr ratios jointly advocate for partial melting of mantle rocks at subduction. However, due to the relatively low LILE and their tholeiitic nature, there is a possibility of mixing with lower crustal material following a very large degree of partial melting.

Generally, magmatic rocks differ in composition and evolution which play a big role in the type of mineralization they host. For instance, U is favorable in veins and anatectic rocks (IAEA 2009), Sn and skarn deposit in igneous rocks (Meinert 1995), while Ni–Cu–PGEs are mantle derived and occur in mafic and ultramafic rocks (Arndt et al. 2005). Based on previous reports (Naldrett 1989, 2004; Naldrett et al. 2013), for all magmatic related mineralization, the key to determine their petrogenesis lies in the understanding of the processes involved in magmatic differentiation. Depending on how depleted the source is (mantle or crust), this can be observed from the petrochemical composition of the resulting rocks. The host lithologies often display characteristic features that commonly serve as guides for future exploration works as the case with the Somies-Ntem lithologies (Table 4).

5.5 Metallogenic significance

Several mapping proxies, fluid pathways and traps related to mineralization of the Somie-Ntem area have been discussed in the previous sections. Based on SiO_2 versus Zn, SiO_2 versus Fe_2O_3(T), SiO_2 versus K/Rb, Ba–Rb–Sr plots (Fig. 9a–d), the mesocratic granites appear to be less productive in the area but host fertile aplite dykes with U-Th

Table 4 Summary table for lithologies within the study area and petrochemical characteristic associated to mineralization

Enriched lithology	Sample code	Mineralization	Mineral assemblage in rocks		Structures		Other chemical features	
			Main	Accessory	Macro	Micro	Major	Trace
Leucogranites	B137, B143, B144, B145	Sn-Zn	High quartz, k-feldspar, plagioclase, aegirine, arfvedsonite,	Casseterite, tourmaline, titanite	Vugs, mafic dykes	Granophires, perthite	High SiO_2, Al2O3, Na_2O, K_2O Very low in MgO, CaO and P_2O_5	High Ag, Hf, Nb, Ta, Y and Cr; Th/U, Sm/Eu, Very low Ba and Sr
Mesocratic aplite dyke	B136	U-Th	Quartz, k-feldspars, plagioclase, biotite	titanite, zircon	Quartz veins, aplite dykes	Quartz veins, fractures	N/A	Cu, Pb
Hornblende-bearing gneisses	B155, B156, B159, B180	Cr-Cu-Ni-V	Plagioclase, hornblende	Olivine, titanite, zircon, opaque minerals	Fractures, veins	Fracture, veinslets	High Fe_2O_3 and CaO Low SiO_2	Mg, Sc, Ti, High Ni/Cu, very low Rb/Sr

mineralization. The source and emplacement of these Pan-African granites in Cameroon are connected to events relating to the geodynamic evolution of the Pan-African belt in Central Africa and, specifically, the continent–continent collision between the north-central Cameroon active margin from the north and the Congo Craton from the south (Toteu et al. 2004). This collision resulted in the subduction of the cratonic plate while the asthenospheric upwelling induced the melting of the crust and granitization, thus explaining the abundance of post-collisional granite within the WCD and AYD relative to the YD (Toteu et al. 2004). However, the Somie-Ntem mesocratic granites show syn- to late collisional settings (Fig. 8c). According to reports, granites within the WCD were derived from the reworking of Paleoproterozoic crust (Toteu et al. 2004; Makitie et al. 2019). These Paleoproterozoic rocks constitute the entire basement of the study area. Based on U–Pb dating on zircon, the granites show an age between 660 and 600 Ma (Makitie et al. 2019). This period either corresponds to sinistral shear deformation (Ngako et al. 2008; Ntieche et al. 2017; Yannah 2020; Fozing et al. 2021) or the transition from crustal thickening (630–610 Ma) and shear zone development in the region (610–540 Ma) (Ngako 1986; Ferré et al. 2002; Tetsopgang et al. 2008; Kwékam et al. 2020a).

Studies on the magnetic susceptibility of granitic rocks show their direct relation to the oxygen fugacity $f(O_2)$ of the igneous system, which in turn plays a crucial role in ore formation (Ishihara 1977; Blevin and Chappel 1995; Maulana et al. 2013). Although visible crystals of magnetite were not observed in hand samples and outcrops in the mesocratic granites, they show characteristics of magnetite series granites due to the strong response they gave to the magnetic pen. Magnetite could equally form part of the opaque phases observed in thin sections. However, reports from Dschang, Misajé and Nkambe areas west of the Tikar plain (Tetsopgang et al. 2006; Kwékam et al. 2020a; Fozing et al. 2021) identified different facies of magnetite series granites bearing medium to megacryst magnetite crystals. Meanwhile measured magnetic susceptibility of granites NW of the study area show $> 3 \times 10^{-3}$ SI for the oxidized type and $< 3 \times 10^{-3}$ for the ilmenite or reduced type (Fozing et al. 2021). These features globally show the similarity in their sources and evolution. Considering that magnetite generally forms accessory phases in magmatic rocks, Pilchin (2010) indicated that magmatic iron generally occurs as ferrous oxides (FeO) in the magma chamber and later transformed and concentrated into the ferric type during magma cooling. This transformation depends on the magmatic activity and the amount of volatiles present (Pilchin 2010). Furthermore, the amount of Mg, Ca, Ti, and Al contents coupled with the temperature, pressure and redox condition controlled this transformation (Pilchin 2010). Nevertheless, the mesocratic (oxidized) granites appear to be barren in the area even though their magnetic character makes them suitable for sulphide mineralization like Fe, Cu, Pb, Zn and Mo (Fozing et al. 2021). Considering that magnetite series granites indicate an oxidized mafic source (Maulani et al. 2013), the infertile nature can be attributed to low hydrothermal input based on the high $K/Rb > 100$ and $Zr/Hf > 20$ ratios and the paucity of magnetite crystals in the rocks. Meanwhile, Fozing et al. (2021) attributed this to Paleoproterozoic crustal reworking that hindered hydrothermal fluid circulation and concentration of ores in the rocks. Nevertheless, a closed observation of the transition of tectonic events in the WCD and AYD shows that there was a significant change in the regional shortening direction from WNW-ESE (D_1-D_2 events) to NNE-SSW directions (D_3 event) and back to WNW-ESE (D_4 event) (Toteu et al. 2004). These changes in stress direct generated rigid blocks that may have caused significant obstruction to tectonic movement in the region (Toteu et al. 2004) and the circulation of hydrothermal fluid for ore deposits. This may explain why most post-collisional granites show low productivity, and their K/Rb ratios are often high.

On the other hand, the Sn-Zn-bearing leucogranites show characteristics of reduced granites based on the weak- to no response they gave to the magnetic pen. They also display very low Mg/Fe ratios relative to the mesocratic granites (Ishihara 1977). As indicated before, they most likely constitute the family of reduced granites within the WCD emplaced in NE-SW structures that were reactivated during crustal extension or D_4 brittle movement that dates 523 ± 35 Ma (Tetsopgang et al. 1999; Toteu et al. 2004; Fozing et al. 2014; Ntieche et al. 2017). Meanwhile, recent reports from U–Pb dating on zircon show the emplacement age of the Tikar plain leucogranites at 57 ± 1 Ma (Makitie et al. 2019). This age corresponds to the period of Cameroon volcanic line plutonism (Kinnaird et al. 2016; Makitie et al. 2019). Their aluminium saturation index shows peraluminous I- to slightly S-type affinity (Fig. 4). Peraluminous leucogranites are generally supersaturated in fluids (H_2O, Cl, F), and undergo significant hydrothermal alteration with metal concentrations of Sn–W–Mo, Pb–Zn–Cu, Au, U, Nb and Ta. Their magmas, of purely crustal origin, are derived from materials that are either orthoderivative (orthogneiss) or paraderivative (sedimentary) materials. According to Maulana et al. (2013), ilmenites series granites with I-type character indicate a high involvement of carbon as a redox agent during magma generation causing reduction and the formation of I-type ilmenites series granites. This suggests some assimilation of sedimentary materials containing high amounts of carbon (Maulana et al. 2013) into the Somie-Ntem leucogranites magma and can be justified by the presence of metasedimentary units within the domain. However, these granites may have the same source as those reported in Bamenda, Nkambe and Misajé (Fozing et al. 2014; Kouankap Nono et al. 2018) but underwent different paths of magma differentiation and emplacement time based on their similarity in composition. Although there is a high possibility that the Somie-Ntem leucogranites are coeval with aplite dyke formation in the study area.

A close comparison between the different veins and dykes in the study area shows that they differ in composition and texture. For instance, the barren dykes gave no magnetic response in the samples and appear in pink and white. The U-Th mineralized dyke, on the other hand, gave a magnetic response slightly weaker than the host mesocratic granite and generally appears grey to dark grey. These characteristics, together with the proxies discussed in the previous sections, could either mean the following: (1) the barren dykes were derived from crustal fluids that form part of the melt involved in the emplacement of leucogranites in the region but experienced different levels of modification during crystallization; (2) during the formation of the mineralized dyke, there was enough time for the melt to interact with the host rock leading to exchange of material and remobilization of U and Th; (3) The enriched melt belongs to an earlier post magmatic event that was remobilized during shear transition from D_2 to D_3 events. Thus in terms of ore potential, focus should be on the aplite dyke appearing grey and weak to moderately magnetic. These observations support the effect of melt hybridization in U-Th mineralization in the area.

Cu–Cr–Ni–V mineralization is hosted by amphibolites and hornblende-bearing gneisses (or banded amphibolites, Fozing et al. 2019). These lithologies form part of the Paleoproterozoic basement within the Tikar plain composed of amphibolites, metabasites and tonalite-trondhjemite-granodiorite (TTG) suite that dates 2.18–2.14 Ga (Tchameni et al. 2001; Toteu et al. 2004; Makitie et al. 2019). Makitie et al. (2019) indicated that the Paleoproterozoic basement north of the CCSZ corresponds to the age of juvenile crustal formation (2180–2140 Ma) when compared to that south of the shear zone in the Linte area (2140–2070 Ma). These mafic bodies most likely form the source of magnetite series granites in the area (Maulana et al. 2013; Fozing et al. 2021). Based on Makitie et al. (2019), there is no continuation of Cu–Cr–Ni–V mineralization in the south within the Linte area, suggesting that the mineralization may be limited within the older Paleoproterozoic crust. Even though it is not clear whether the presence of these metals signifies a porphyry sulfide or Cu–Ni–PGEs deposits in the region, it is possible that the mineralization is syn-genetic and was remobilized during shear deformation.

6 Conclusions

The Somie-Ntem area consists of metaluminous and peraluminous I- to slightly S-type granitoids. They also show high-K calc-alkaline to shoshonite affinity. However, the physical properties of the rocks show that the mesocratic granites belong to the magnetite series (oxidized) while the leucogranites to the ilmenite series (reduced) granites. The leucogranites with the reduced character are younger than the mesocratic, post-orogenic intraplate setting and show high productivity for Sn–Zin mineralization based on the Sm/Eu ratio, Ba–Rb–Sr, Fe_2O_3(T) versus SiO_2 and Zn versus SiO_2 proxies. Although they show similarity to most ilmenite granites within the region, their high productivity for Sn-Zn is firmly due to postmagmatic metasomatism, greisenization and the presence of volatiles owing to their intense granophyric structures. Based on field relationships and similar low magnetic susceptibility, their age is most likely coeval to the emplacement of the aplite dykes that crosscut the mesocratic granites. However, some dykes may have experienced melt hybridization to concentrate U–Th mineralization.

The mesocratic granites show a syn-collisional setting, but they appear barren even though their oxidized character shows their mafic origin and makes them suitable for sulphide mineralization. Cu–Cr–Ni–V mineralization in amphibolites and hornblende-bearing gneisses forms part of the mafic Paleoproterozoic suites within the domain. This mineralization may either indicates a sulphide deposit or a plausible Cu–Ni–PGEs deposite. Nevertheless, the mineralization is most likely syn-genetic that suffered some modification from shear deformation and weathering. In general, hydrothermal contribution to mineralization in the region is limited based on the consistently high K/Rb $>$ 100 and Zr/HF $>$ 20 in the rocks. A major cause of infertility of these rocks could be the changes in stress direction during shear deformation from WNW-ESE (D_1–D_2) to NNE-SSW (D_3) and back to WNW-ESE (D_4) direction. These changes did obstruct tectonic movement in the region and hindered hydrothermal activity and thus low productivity of the rocks.

Supplementary Information The online version contains supplementary material available at https://doi.org/10.1007/s11631-022-00552-z.

Acknowledgements The authors wish to appreciate the financial support that was provided to the corresponding author by the capacity building project in the mining sector (PRECASEM) under the Ministry of Mines, Industries and Technological Development of Cameroon to carry out the field work for this study.

Author contributions On behalf of all authors of this work, I hereby declare that this work has received contribution from all authors listed. The fieldwork was done by the corresponding [MY], the second [YF] and firth authors [TAJ]. The corresponding author wrote the first draft and this was corrected by MK, KDA, ASN, BJM. The final work was read and approved by all authors.

Funding I declare that no direct funding was obtained for this work. However, the fieldwork was done under the capacity building project in the mining sector (with French acronym PRECASEM) under the Ministry of Mines; Industries and Technological Development of Cameroon.

Declarations

Conflict of interest The authors declare that they have no conflicting interest be it financial or personal relationships that could influence the publication of this paper.

References

Archanjo CJ, Bouchez JL (1991) Le Sérido, une chaîne transpressive dextre au Proterozoïque supérieur du Nord-Est du Brésil. Bulletin De La Société Géologique De France 162:637–647

Arndt N, Lesher CM, Czamanske GK (2005) Mantle-derived magmas and magmatic Ni–Cu–(PGE) deposits. Econ Geol 100:5–24

Bahajroy M, Taki S (2014) Study of the mineralization potential of the intrusives around Valis (Tarom-Iran). Earth Sci Res J 18:123–129

Bambi CKM, Suh CE, Nzenti JP, Frimmel HE (2012) U-Mo mineralization potential in Pan-African granites, southwestern Cameroon: Economic geology of the Ekomédion prospect. J Afr Earth Sci 65:25–45

Banaś M, Mochnacka K (1986) Two uranium deposits in the Polish part of the Sudety Mountains. International Atomic Energy Agency Technical. Documents 361:335–358

Banaś M, Mochnacka K (1989) Genetic types of uranium mineralization in Poland and their metallogenic relationships. In: Metallogenesis of uranium deposits, panel proceedings series, International Atomic Energy' Agency, Vienna, pp 187–200

Barker SD (1970) Compositions of granophyre, myrmekite and graphic granite. Geol Soc Am Bull 81:3339–3350

Barnes SJ, Cruden AR, Arnd N, Saumur BM (2016) The mineral system approach applied to magmatic Ni-Cu-PGE sulphide deposits. Ore Geol Rev 76:296–316

Batchelor RA, Bowden P (1985) Petrogenetic interpretation of granitoid rocks series using multicationic parameters. Chem Geol 48:43–55

Bea F (1996) Residence of REE, Y, Th and U in granites and crustal protoliths; implications for the chemistry of crustal melts. J Petrol 37:521–552

Bea F, Montero P, Ortega M (2006) A LA-ICP-MS evaluation of Zr reservoirs in common crustal rocks: implications for Zr and Hf geochemistry, and zircon forming processes. Can Miner 44:693–714

Begg GC, Hronsky JAM, Arndt NT, Griffin WL, O'Reilly SY, Hayward N (2010) Lithospheric, cratonic and geodynamic setting of Ni–Cu–PGE sulfide deposits. Econ Geol 105:1057–1070

Beus AA (1968) Geochemical criteria in theoretical principles of exploration for mineral deposits, Moscow, pp 127–145

Beus AA, Severov EA, Sitnin AA, Subbotin KD (1962) Albitized and greisenized granite (apogranite). Izvestija Akademii Nauk SSSR, Moscow (**in Russian**)

Blevin P (2003) Metallogeny of granitic rocks. In: Blevin P et al. (eds) Magmas to mineralization. The Ishihara symposium, pp 1–4

Blevin PL, Chappell B (1995) Chemistry, origin, and evolution of mineralized granites in the Lachland Fold Belt, Australia; the metallogeny of I and S-type granites. Econ Geol 90:1604–1619

Bonin B (1990) From orogenic to anorogenic setting: evolution of granitic suites after a major orogenesis. Geol J 25:261–270. https://doi.org/10.1002/gj.3350250309

Cerny P (1971) Graphic intergrowths of feldspars and quartz in some Czechoslovak pegmatites. Contrib Miner Pet 30:343–355

Cerny P, Burt DM (1984) Paragenesis, crystallochemical characteristics and geochemical evolution of micas in granitic pegmatites.

In: Bailey SW (ed) Micas, mineralogical society of america review. Mineral, Chantily, vol 13, pp 257–297

Černý P, Goad BE, Hawthorne C, Chapman R (1986) Fractionation trends of the Nb-and Ta-bearing oxide minerals in the Greer Lake pegmatite granite and its pegmatite aureole, southeastern Manitoba. Am Miner 71:501–507

Chappell BW, White AJR (1992) I- and S- type granites in the Lachlan Fold Belt. Trans R Soc Edinb Earth Sci 83:1–26

Chappell BW, Bryant CJ, Wyborn D, White AJR, Williams IS (1998) High- and low-temperature I-type granites. Ressour Geol 48:225–235. https://doi.org/10.1111/j.1751-3928.1998.tb00020.x

Chetty D, Frimmel HE (2000) The role of evaporites in the genesis of base meta- sulphide mineralization in the Northern Platform of the Pan-African Damara Belt, Namibia: geochemical and fluid inclusion evidence from carbonate wall rock alteration. Miner Deposita 35:364–376

Cox KG, Bell JD, Pankhurst RJ (1979) The interpretation of igneous rocks. Allen and Unwin, London. https://doi.org/10.1007/978-94-017-3373-1

Dawaï D, Bouchez JL, Paquette JL, Tchameni R (2013) The Pan-African quartz-syenite of guider (north-Cameroon): magnetic fabric and U-Pb dating of a late orogenic emplacement. Precambrian Res 236:132–144

Dekking FM, Kraaikamp C, Lopuhaä HP, Meester LE (2005) A modern introduction to probability and statistics. Springer texts in statistics. Springer, London. https://doi.org/10.1007/1-84628-168-7. ISBN 978-1-85233-896-1

Dini A, Rocchi S, Westerman DS (2004) Reaction micro textures of REE-Y-Th-U accessory minerals in the Monte Capanne Pluton (Elba Island, Italy): a possible indicator of hybridization processes. Lithos 78:101–118

Djouka-Fonkwé M, Schulz B, Schüssler U, Tchouankoué JP, Nzolang C (2008) Geochemistry of the Bafoussam Pan-African I and S-type granitoids in western Cameroon. J Afr Earth Sci 50:148–167

Dostal J, Chatterjee AK (2000) Contrasting behavior of Nb/Ta and Zr/Hf ratios in a peraluminous granitic pluton (Nova Scotia, Canada). Chem Geol 163:207–218

Duuring P, Rowins SM, McKinley BSM, Dickinson JM, Diakow LJ, Kim YS, Creaser R (2009) Magmatic and structural controls on porphyry-style Cu-Au-Mo mineralization at Kemess South, Toodoggone District of British Columbia, Canada. Miner Deposita 44:435–462

Ekwere SJ (1985) Li, F and Rb contents and Ba/Rb and Rb/Sr ratios as indicators of postmagmatic alteration and mineralization in the granitic rocks of the Banke and Ririwai Younger Granite complexes, Northern Nigeria. Miner Deposita 20:89–93

El Gharbawy RI, El Maadawy WM (2012) Geochemistry of the uranium-thurium-bearing granitic rocks and pegmatites of Wadi Haleifiya area, Southeastern Sinai. Egypt Chin J Geochem 31:242–259

Ferré E, Déléris J, Bouchez JL, Lar AU, Peucat JJ (1996) The Pan-African reactivation of Eburnean and Archean provinces in Nigeria: structural and isotopic data. J Geol Soc London 153:719–728

Ferré E, Gleizes G, Caby R (2002) Obliquely convergent tectonics and granite emplacement in the Trans-Saharan belt of Eastern Nigeria: a synthesis. Precambrian Res 114:199–219

Fouquet Y, Cambon P Etoubleau J, Charlou JL, Ondréas H, Barriga FJAS, Cherkashov G, Semkova T, Poroshina I, Bohn M, Donval JP, Henry K, Murphy P, Rouxel O (2010) Geodiversity of hydrothermal processes along the mid-Atlantic ridge and ultramafic-hosted mineralization: a new type of oceanic Cu–Zn–Co–Au volcanogenic massive sulfide deposit. In: Rona PA, Devey CW, Dyment J, Murton BJ (eds) Diversity of hydrothermal systems on slow spreading ocean ridges. American Geophysical Union, pp 321–367

Fozing EM, Kwékam M, Njanko T, Njonfang E, Séta N, Yakeu Sandjo AF et al (2014) Structural evolution of the Pan-African Misajé pluton (Northwestern Cameroon). Syllab Rev Sci Ser 5:12–26

Fozing EM, Kwékam M, Gountié Dedzo M, Asaah Asobo NE, Njanko T, Tcheumenak Kouémo J et al (2019) Petrography and geochemistry of amphibolites from the Fomopéa Pluton (West Cameroon) origin and geodynamic setting. J Afr Earth Sci 154:181–194. https://doi.org/10.1016/j.jafrearsci.2019.03.024

Fozing EM, Kwékam M Tetsopgang S, Njanko T, Chako-Tchamab B, Tcheumenak Kouémo J, Gountie Dedzo M, Asobo Nkengmatia EA, Njiki Chatu C (2021) The mineralization potential of the I-type granites from Misaj_e pluton (NW-Cameroon): AMS and geochemical constraints. Solid Earth Sci

Frost BR, Barnes CG, Collins WJ, Arculus RJ, Ellis DJ, Frost CD (2001) A geochemical classification for granitic rocks. J Pet 42:2033–2048

Gajda E (1960a) Minerals of pegmatite veins in the vicinity of Szklarska Poręba region in the Karkonosze Mts. Kwartalnik Geologiczny 4:565–585

Gajda E (1960b) Pegmatite veins of the region of Szklarska Poręba, (Karkonosze Mts). Kwartalnik Geologiczny 4:545–546

Gerdes A, Montero P, Bea F, Fershater G, Borodina N, Osipova T, Shardakova G (2002) Peraluminous granites frequently with mantle-like isotope compositions: the continental-type Murzinka and Dzhabyk batholiths of the eastern Urals. Int J Earth Sci 91:3–19

Ghodsi MR, Boomeri M, Bagheri S, Lentz D, Ishiyama D (2016) Metallogeny and mineralization potential of the Bazman Granitoids. SE Iran Resour Geol 66:286–302

Girei MB, Li H, Algeo TJ, Bonin B, Ogunleye PO, Buteh S, Ahmeddi HA (2019) Petrogenesis of A-type granites associated with Sn-Nb-Zn mineralization in Ririwai complex, north-Central Nigeria: constraints from whole-rock SmNd and zircon Lu, Hf isotope systematics. Lithos 341:49–70

Gomes MEP, Neiva AMR (2002) Petrogenesis of tin-bearing granites from Ervedosa, Northern Portugal: the importance of magmatic processes. Chemie Der Erde Geochem 62:47–72

González FJ, Somoza L, Hein JR, Medialdea T, León R, Urgorri V, Reyes J, Martín-Rubí JA (2016) Phosphorites, Co-rich Mn nodules, and Fe–Mn crusts from Galicia Bank, NE Atlantic: reflections of Cenozoic tectonics and paleoceanography. Geochem Geophys Geosyst 17:346–374

Goswami B, Bhattcharyya C, Basak A, Mukherjee G, Emporto C, Tripathi S (2015) Petrography and geochemistry of aegirine-arfvedsonite bearing granite gneiss from Dimra Pahar, Hazaribagh District, Jharkhand, eastern India: implication for petrogenetic evolution. In: Conference: international conference on research development in environment, social sciences and humanities at: University of Delhi (DU), Conference Centre, New Delhi (India), pp 108–122

Govett GJS, Atherden PR (1988) Application of rock geochemistry to productive plutons and volcanic sequences. Geochem Explor 30:223–242

Grenholm M (2011) Petrology of Birimian granitoids in southern Ghana-petrography and petrogenesis. Kandidatuppsats I Geologi vid Lunds Universitet, nr. 285

Groves DI, McCarthy TS (1978) Fractional crystallization and the origin of tin deposits in granitoids. Miner Deposita 3:11–26

Haapala I (1977) The controls of tin and related mineralization in the rapakivi-granite areas of south-eastern Fennoscandia. Geol Fören Stockh Förh 99:130–142

Haapala I (1995) Metallogeny of the rapakivi granites. Mineralogy and servations on the melt inclusions. Reimar Seltmann, Petrology 54:141–160

Haapala I (1997) Magmatic and postmagmatic processes in tin-mineralized granites: topaz-bearing leucogranite in the Eurajoki rapakivi granite stock, Finland. J Pet 38:1645–1659

Harris NBW, Marzouki FMH, Ali S (1986) The Jabel Sayid complex, Arabian Shield: geochemical constraints on the origin of peralkaline and related granites. J Geol Soc London 143:287–295

Hein JR, Schulz MS, Dunham RE, Stern RJ, Bloomer SH (2008) Diffuse flow hydrothermal manganese mineralization along the active Mariana and southern Izu-Bonin arc system, western Pacific. J Geophys Res 113:B08S14. https://doi.org/10.1029/2007jb005432

Horbe MA, Horbe AC, Costi HT, Teixeira JT (1991) Geochemical characteristics of cryolite-tin bearing granites from the Pitinga Mine, northwestern Brazil—a review. J Geochem Explor 40:227–249

Hrouda F, Chlupacova M, Chadima M (2009) The use of magnetic susceptibility of rocks for geological exploration. Georadis

IAEA (2009) World Distribution of Uranium Deposits (UDEPO) with Uranium Deposit Classification. IAEA, Vienna, IAEA-TEC-DOC-1629, 117 p

Ibrahim ME, Saleh GM, Abd El-Naby HH (2001) Uranium mineralization in the two mica granite of Gabal Ribdab area, South Eastern Desert. Egypt Appl Radiat Isot 55:861–872

Imeokparia EG (1981) Ba/Rb and Rb/Sr ratios as indicators of magmatic fractionation, postmagmatic alteration and mineralization Afu Younger Granite Complex, Northern Nigeria. Geochem J 15:209–219

Imeokparia EG (1983) Geochemical aspects of the evolution and mineralization of the Amo Younger Granite Complex (northern Nigeria). Chem Geol 40:293–312

Imeokparia EG (1985) Rare-metal mineralization in granitic rocks of Tongolo Anorogenic Complex, Northern Nigeria. Miner Deposita 20:81–88

Imeokparia EG (1990) The Shere igneous Complex, central Nigeria: geochemical constraints on the origin of peralkaline and associated granites. Geologic En Mujinbow 69:121–131

Imeokparia EG (1993) Geochemical aspects of the evolution and mineralization of the Amo Younger Granite Complex (northern Nigeria). Chem Geol 40:293–213

Ishihara S (1977) The magnetite-series and ilmenite-series granitic rocks. Min Geol 27:293–305

Janoušek V, Farrow CM, Erban V (2006) Interpretation of whole-rock geochemical data in igneous geochemistry: introducing geochemical data toolkit (GCDkit). J Pet 47:1255–1259

Kanasiewicz J (1988) Aktualne wyniki poszukiwań mineralizacji związanych z kompleksem skał zasadowych w rejonie niecki żytawskiej. Kwartalnik Geologiczny (in Czech) 32:213–214

Karimpour MH, Bowes WW (1983) Application of trace elements and isotopes for discriminating between porphyry molybdenum, copper, and tin systems and the implications for predicting the grade. Glob Tecton Metallog 2:29–36

Kinnaird JA (1985) Hydrothermal alteration and mineralization of the alkaline orogenic ring complexes of Nigeria. J Afr Earth Sci 3:229–251

Kinnaird JA, Nex PAM, Milani L (2016) Tin in Africa. Episodes 39:361–380

Kouankap Nono GB, Wotchoko P, Ganno S, Njinchuki DN, Nzenti JP, Suh CE (2013) Petrochemical characterization of two distinct types of dolerites from Bafoussam Area, West Cameroon. Int J Geosci 4:1131–1144

Kouankap Nono GD, Wotchoko P, Magha A, Ganno S, Njoya N, Ngambu AA, Nzenti JP, Kabeyene VK (2018) Contrasting Ba-Sr Granitoids from Bamenda Area, NW Cameroon: sources characteristics and implications for the evolution of the Pan African Fold Belt. J Geosci Geomat 6:65–76

Kouske AP, Suh CE, Ghogomu RT, Ngako V (2012) Na-Metasomatism and uranium mineralization during a two-stage albitization at Kitongo, Northern Cameroon: structural and geochemical evidence. Int J Geosci 3:258–279

Kovalenko VI (1978) The genesis of rare metal granitoids and related ore deposits. In: Stemprok M, Burnol L, Tischendorf G (eds) Metallization associated with acid magmatism. Geological Survey, Prague, vol 3, pp 235–247

Kretz R (1983) Symbols of rock–forming minerals. Am Miner 68:277–279

Kretz R, Hartree R, Jones P (1989) Metasomatic crystallization of muscovite in granite and tourmaline in schist related to pegmatite emplacement near Yellowknife, Canada. Contrib Mineral Petrol 102:191–204

Kuhn T, Bostick BC, Koschinsky A, Halbach P, Fendorf S (2003) Enrichment of Mo in hydrothermal Mn precipitates: possible Mo sources, formation process and phase associations. Chem Geol 199:29–43

Kwékam M, Istvan Dunkl I, Fozing EM, Gerald HG, Njanko T, Tcheumenak Kouémo J, Njonfang E (2020a) Syn-kinematic ferroan high-K I-type granites from Dschang in southwestern Cameroon: UePb age, geochemistry and implications for crustal growth in the late Pan-African orogeny. J Geol Soci London. https://doi.org/10.1144/SP502-2019-19

Kwékam M, István Dunkl I, Fozing EM, Gerald HG, Njanko T, Tcheumenak Kouémo J, Njonfang E (2020b) Syn-kinematic ferroan high-K I-type granites from Dschang in southwestern Cameroon: U-Pb age, geochemistry and implications for crustal growth in the late Pan-African orogeny. J Geol Soc London. https://doi.org/10.1144/SP502-2019-19

Kwékam M, Talla V, Fozing EM, Tcheumenak Kouémo J, Dunkl I, Njonfang E (2020c) The Pan-African High-K I-Type Granites From Batié Complex, West Cameroon: age, origin, and tectonic implications. Front Earth Sci 8:363

Kyser K (2014) Uranium ore deposits. In: Holland HD, Turekian KK (eds) Treatise on geochemistry, 2nd edn. Elsevier, pp 489–513

Le Marechal A (1975) Carte géologique de l'Ouest du Cameroun et de l'Adamaoua. Office de la Recherche Scientifique et Technique Outre-Mer (ORSTOM), Service Central de documentation, pp 70–74, Route d'Aulnay-93 Bondy France

Lentz D (1996) U, Mo, and REE mineralization in late tectonic granitic pegmatites, southwestern Grenville Province. Ore Geol Rev 11:197–227

Lesher CM (1989) Komatiite-associated nickel sulfide deposits. In Whitney JA, Naldrett AJ (eds) Ore deposition associated with magmas. Society of Economic Geologists, pp 45–102

Li P, Liang T, Feng Y, Zhao T, Tian J, Li D, Li J, Chen G, Wu G (2021) The metallogeny of the Lubei Ni–Cu–Co sulfide deposit in Eastern Tianshan, NW China: insights from petrology and Sr–Nd–Hf isotopes. Earth Sci Front 9:1–17

Lightfoot PC, Hawkesworth CJ (1997) Flood basalts and magmatic Ni, Cu and PGE sulphide mineralization: comparative geochemistry of the Noril'sk (Siberian Trap) and West Greenland Sequences. Am Geophys Union Monogr 100:357–380

Linnen RL (1998) The solubility of Nb-Ta-Zr-Hf-W in granitic melts with Li and Li + F: constraints for mineralization in rare metal granites and pegmatites. Econ Geol Bull Soc Econ Geol 93:1013–1025

Linnen RL, Keppler H (2002) Melt composition control of Zr/Hf fractionation in magmatic processes. Geochim Cosmochim Acta 66:3293–3301

Linnen RL, Van Lichtervelde M, Cerny P (2012) Granitic pegmatites as sources of strategic metals. Elements 8:275–280

London D (2008) Pegmatites. Can Miner 10:1–347

Makitie H, Baptiste J, Yannah M, Tucker VR, Houketchang Bouyo M, Bernard J, Karinen T, Vic G, Fodoue Y, Sep Nlomngan JP, Wongolo Djombol MH, Moussango Ibohn P, Tchokona Seuwui D (2019) Carte géologique à 1/200 000 de la République du Cameroun—Feuille BANYO (NB-32-XVII). 1ère édition. Editeur: Ministère des Mines, de l'Industrie et du Développement Technologique du Cameroun, Yaoundé

Marks M, Vennemann T, Siebel W, Markl G (2003) Quantification of magmatic and hydrothermal processes in a peralkaline syenite-alkali equilibria, and radiogenic isotopes. J Pet 44:1247–1280

Markwitz V, Hein KAA, Jessell MW, Miller J (2016) Metallogenic portfolio of the West Africa Craton. Ore Geol Rev 78:558–563

Matos JX, Ferrero A, Gatley S, Pereira1 Z, Préteseille S, Sánchez A, Marchán C, Sánchez A, Díaz-Martínez E, Hughes S, Tippings A, Cayla P, Morris JH (2012) Geological heritage and land valorization in mining regions-the Atlanterra Atlantic Area best examples. In: Atlanterra international congress meeting Nantes 2012.

Maulana A, Watanabe K, Imai A, Yonezeu K (2013) Origin of magnetite and ilmenite-series granitic rocks in Sulawesi, Indonesia: magma genesis and regional metallogenic constraint. Procedia Earth Planet Sci 6:50–57

Mbassa BJ, Njonfang E, Grégoire G, Itiga Z, Kamgang P, Benoit M, Ndjigui PD, Ngwa CN, Nolla JD (2018) Evaluation of the mineralizing potential of the Mbengwi plutons, Northwestern Cameroon, Central Africa. Arab J Geosci 11:657

McCarthy TS, Hasty RA (1976) Trace element distribution pattern and their relationship to the crystallization granitic melts. Geochim Cosmochim Acta 40:1351–1358

McKechnie CL, Annesley IR, Ansdell K (2012) Radioactive abyssal granitic pegmatites and leucogranites in the Wollaston Domain, northern Saskatchewan, Canada: mineral compositions and conditions of emplacement in the Fraser Lakes area. Can Miner 50:1637–1667

McKechnie CL, Annesley IR, Ansdell K (2013) Geological setting, petrology and geochemistry of granitic pegmatites hosting the Fraser Lakes Zone B U-Th–REE mineralization, Wollaston Domain, northern Saskatchewan, Canada. Explor Min Geol 21:1–26

Mckeough MA, Lentzd R, Chris RM, Mcfarlane CRM, Brown J (2013) Geology and evolution of pegmatite-hosted U-Th $\pm$ REE-Y-Nb mineralization, Kulyk, Eagle, and Karin Lakes region, Wollaston Domain, northern Saskatchewan, Canada: examples of the dual role of extreme fractionation and hybridization processes. J Geosci 58:321–346

Meinert LD (1995) Compositional variation of igneous rocks associated with skarn deposits—chemical evidence for a genetic connection between petrogenesis and mineralization. In: Thompson JFH (ed) Magmas fluids and ore deposits. Mineralogical Association of Canada Short Course Series, vol 23, pp 401–418

Montes-Lauar CR, Trompette R, Melfi AJ, Bellieni G, De Min A, Béa A, Peccerillo EM, Affaton P, Pacca IG (1997) Pan-African Rb–Sr isochron of magmatic rocks from northern Cameroon. Preliminary results. In: South American symposium on isotope geology, Brazil, pp 204–205

Morgan GB, London D (2012) Process of granophyre crystallization in the Long Mountain Granite, southern Oklahoma. Geol Soc Am Bull 124:1251–1261

Mungall JE (2007) Magmatic ore deposits. In: Rudnick R (ed) The crust-Treatise on geochemistry, vol 3, chapter 21. Elsevier, p 133

Nabelek PI, Whittington AG, Sirbescu MLC (2010) The role of H_2O in rapid emplacement and crystallization of granite pegmatites: resolving the paradox of large crystals in highly undercooled melts. Contrib Miner Pet 160:313–325

Naldrett AJ (1973) Nickel sulphide deposits-their classilication and genesis, with special emphasis on deposits of volcanic association. Bull Can Inst Minins Met 66:45–61

Naldrett AJ (1989) Introduction: magmatic deposits associated with mafic rocks. In: Whitney JA, Naldrett AJ (eds) Ore deposition associated with magmas. Society of Economic Geologists, pp 1–3

Naldrett AJ (1999) World-class Ni–Cu–PGE deposits: key factors in their genesis. Miner Deposita 34:227–240

Naldrett AJ (2004) Magmatic sulfide deposits: geology, geochemistry, and exploration. Springer

Naldrett AJ (2013) Magmatic sulfide deposits: geology, geochemistry and exploration. Springer, Berlin. https://doi.org/10.1007/s001260050200

Naldrett AJ, Kinnaird JA, Wilson A, Yudovskaya M, McQuade S, Chunnett G, Stanley C (2009) Chromite composition and PGEcontent of Bushveld chromitites: part 1-the lower and middle groups. Appl Earth Sci 118:131–161

Negue NE, Tchameni R, Vanderhaeghe O, Fenguye S, Barbey P, Tekoum L, Eglinger A, Fosso Tchunte PM, Saha FAN (2017) Structure and LA-ICP-MS zircon U-Pb dating of syntectonic plutons emplaced in the Pan-African Banyo-Tcholliré shear zone (Central North Cameroon). J Afr Earth Sci 131:251–271

Neves BB, Van Schmus WR, Fetter A (2002) North western, Africa-north, east Brazil: major tectonic links and correlation problems. J Afr Earth Sci 34:275–278

Ngako V (1986) Evolution métamorphique et structurale de la bordure Sud-ouest de la "série de Poli" (segment camerounais de la chaîne panafricaine). Mémoires et documents du Centre armericain d'étude structurale des socles, No 5

Ngako V (1999) Les déformations continentales panafricaines en Afrique Centrale: résultat d'un poinconnement de type himalayen. Thèse de doctorat d'Etat (in French), Université de Yaoundé I Cameroon

Ngako V, Njonfang E (2011) Plates amalgamation and plate destruction, the Western Gondwana history. In: Closson D (ed) Tectonics. INTECH, UK

Ngako V, Jegouzo P, Nzenti JP (1992) Champ de raccourcissement et de cratonisation du Nord Cameroun du protérozoïque supérieur au protérozoïque moyen (in French). Comptes Rendu De L'académie Des Sciences De Paris 315:371–377

Ngako V, Affaton P, Njonfang E (2008) Pan-African Tectonics in North western Cameroon: implication for history of Western Gondwana. Gondwana Res 14:509–522

Ngako V, Affaton P, Nnange JM, Njanko TH (2003) Pan-African tectonic evolution in the central and southern Cameroon: transpression and trans-tension during sinistral shear movements. J Afr Earth Sci 36:207–214

Ngo Belnoun RN, Tchouankoué JP, Itiga Z, Wambo NAS, Owona S, Koller F, Thöni M (2006) Geochemistry of the Bayon plutonic complex—Western Cameroon. Global J Geol Sci 111:73–93

Nguéné FR (1982) Geology and geochemistry of the Mayo Darlé tin deposit, West-Central Cameroon. PhD Thesis, New Mexico Institute

Njanko T, Nédélec A, Kwékam M, Siqueira R, Esteban L (2010) Emplacement and deformation of the Fomopéa pluton: implication for the Pan-African history of Western Cameroon. J Struct Geol 32:306–320

Novák M (2007) Contamination in granitic pegmatites; examples from the Moldanubicum, Czech Republic. The State of the Art. In: International symposium. Porto, Portugal, pp 1–4

Novák M, Selway JB, Černý P, Hawthorne FC, Ottolini L (1999) Tourmaline of the elbaite–dravite series from an elbaite-subtype pegmatite at Bližná, southern Bohemia, Czech Republic. Eur J Miner 11:557–568

Ntiéche B, Ram Mohan M, Moundi A, Mounjouohou MA (2016) Petrogenesis and geochemical characterization of the granitoids of the Magba Shear Zone West Cameroon Central Africa. Open J Geol 6:812–839

Ntieche B, Mohan MR, Moundi A (2017) Granitoids of the Magba Shear Zone, West Cameroon, Central Africa: evidences for emplacement under transpressive tectonic regime. J Geol Soc India 89:33–46

Nzenti JP (1998) Neoproterozoic alkaline meta-igneous rocks from the Pan-African North Equatorial Fold Belt (Yaounde, Cameroon): biotites and magnetite rich pyroxenites. J Afr Earth Sci 26:37–47

Nzenti JP, Ngako V, Kambou R, Penaye J, Bassahak J, Njel UO (1992) Régionales de la chaîne panafricaine au Nord-Cameroun. Comptes Rendu De L'académiedes Sciences De Paris 611:115–119

Nzenti JP, Abaga B, Suh CE, Nzolang C (2010) Petrogenesis of peraluminous magmas from the Akum-Bamenda Massif, Pan-African Fold Belt, Cameroon. Int Geol Rev 1:1–29

Nzina AC, Nzenti JP, Njiosseu ELT, Ganno S, Ngnotue T (2010) Synkinematic ferro-potassic magmatism from the Mekwene-Njimafofire Foumban Massif, along the Foumban-Banyo shear zone in central domain of Cameroon Pan-African fold belt. J Geol Min Res 2:142–158

Ogunleyea PO, Ikeb EC, Garba I (2005) Geochemical characteristics of the niobium-rich arfvedsonite granites, Younger Granites province of Nigeria. Chem Erde 65:279–296

Olade MA (1980) Geochemical characteristics of tin-bearing and tin-barren granites, northern Nigeria. Econ Geol 75:71–82

Owen JV (1989) Metasomatically altered amphibolite inclusions in zoned granitic–tonalitic pegmatite near Chicoutimi, Quebec. Can Miner 27:315–321

Pan Y (1997) Controls on the fractionation of isovalent trace elements in magmatic and aqueous systems: evidence from Y/Ho, Zr/Hf, and lanthanide tetrad effect—a discussion of the article by Bau M (1996). Contrib Miner Pet 128:405–408

Pearce JA, Harris NBW, Tindle AG (1984) Trace elements discrimination diagrams for the geotectonic interpretation of granite rocks. J Pet 25:956–983

Peccerillo A, Taylor SR (1976) Geochemistry of Eocene calc-alkaline volcanic rocks from the Kastamonu area, Northern Turkey. Contrib Miner Pet 58:63–81

Pelleter E, Fouquet Y, Etoubleau J, Cheron S, Labanieh S, Josso P, Langlade J (2016) Ni-Cu–Co-rich hydrothermal manganese mineralization in the Wallis and Futuna back-arc environment (SW Pacific). Ore Geol Rev 87:126–146

Penaye J, Toteu SF, Van Schmus WR, Nzenti JP (1993) U-Pb and Sm-Nd preliminary geochronologic data on the Yaounde Series, Cameroon: re-interpretation of the granulitic rocks as the suture of a collision in the '"Central African"' belt. Comptes Rendus Science Academy Paris 317:789–794

Pilchin A (2010) Magnetite: the story of the mineral's formation and stability; Chapter 1. In: Angrove DM (ed) Magnetite: structure, properties and applications. Toronto, Ontario, Canada. Nova Science Publishers, Inc. https://www.researchgate.net/publication/287237583

Post JE (1999) Manganese oxide minerals: crystal structures and economic and environmental significance. Proc Natl Acad Sci 96:3447–3454

Reimann C, Filzmoser P (2000) Normal and log normal data distribution in geochemistry: death of a myth. Consequences for the statistical treatment of geochemical and environmental data. Environ Geol 39:1001–1014

Reimann C, Filzmoser P, Garrett RG (2005) Background and threshold: critical comparison of methods of determination. Sci Total Environ 346:1–16

Rhys D, DiMarchi J, Smith M, Friesen R, Rombach C (2003) Structural setting, style and timing of vein-hosted gold mineralization at the Pogo deposit, east central Alaska. Miner Deposita 38:863–875

Rossi JN, Toselli AJ, Basei MA, Sial AN, Baez M (2011) Geochemical indicators of metalliferous fertility in the Carboniferous San Blas pluton, Sierra de Velasco, Argentina. In: Sial AN et al (eds) Granite-related ore deposits, vol 350. Geological Society, pp 175–186

Saleh GM, Kamar SM (2018) Geochemical characteristics and radioactive elements estimation along trenches of Um Ara area, South Eastern Desert, Egypt. Geoinform Geostat Overv 6:2. https://doi.org/10.4172/2327-4581.1000184

Schulz KJ, Chandler VW, Nicholson SW, Piatak Nadine Seall II RR, Woodruff LG, Zientek ML (2010) Mamatic sulfide-rich nickel-copper deposits related to picrite and (or) tholeiitic basalt dike-sill complexes—a preliminary deposit model. U.S. Geological Survey Open-File Report 2010-1179. Available at http://pubs.usgs.gov/of/2010/1179/

Shearer CK, Papike JJ, Jolliff BL (1992) Petrogenetic links among granites and pegmatites in the Harney Peak rare-element granite-pegmatite system, Black Hills, South Dakota. Can Miner 30:785–809

Shelley D (1966) The significance of granophyric and myrmekitic textures in the Lundy Granites. Miner Mag 35:678–692

Sillitoe RH (1996) Granites and metal deposits. Episodes 19:126–133

Simmons WB, Heinrich EW (1980) Rare-earth pegmatites of the South Platte district, Colorado. Colorado Geological Survey Department of Natural Resources, Resource Series, vol 11, pp 1–138

Simmons WB, Webber KL (2008) Pegmatite genesis: state of the art. Eur J Miner 20:421–438

Stemprok M (1971) Petrochemical features of tin-bearing granites in the Krusne hory Mts. Soc Min Geol Jpn 2:112–118

Stemprok M (1987) Greisenization. Geol Rundsch 76:169–175

Strauss CA (1954) The geology and mineral deposits of the Petgietersrus Tinfields. Geol Surv S Afr 46:241

Suh CE, Lehmann B, Mafany GT (2006) Geology and geochemical aspects of lode gold mineralization at Dimako-Mboscorro, SE Cameroon. Geochem Explor Environ Anal 6:295–309

Taylor RP, Strong DF, Fryer BJ (1981) Volatile control of contrasting trace element distributions in peralkaline granitic and volcanic rocks. Contrib Miner Pet 77:267–271

Tchameni R, Mezger K, Nsifa NE, Pouclet A (2001) Crustal origin of early Proterozoic syenites in the Congo craton (Ntem complex), South Cameroon. Lithos 57:23–42

Tchameni R, Sun F, Dawaï D, Danra G, Tékoum L, Nomo Negue E, Vanderhaeghe O, Nzolang C (2016) Nguihdama Dagwaï6Zircon dating and mineralogy of the Mokong Pan-African magmatic epidote-bearing granite (North Cameroon). Int J Earth Sci 105:1811–1830

Tchunte PMF, Tchameni R, André-Mayer AS, Dakoure HS, Turlin F, Poujol M, Nomo EN, Fouotsa AS, Rouer O (2018) Evidence for Nb–Ta occurrences in the Syn-Tectonic Pan-African Mayo Salah Leucogranite (Northern Cameroon): constraints from Nb–Ta oxide mineralogy, geochemistry and U-Pb LA-ICP-MS. Geochronology on columbite and monazite. Minerals 8:188

Tetsopgang S, Enami M, Njonfang E (2006) Petrology of highly evolved Pan-African two-mica granites from the Nkambe area, West Cameroon. J Afr Earth Sci 46:305–317

Tetsopgang S, Suzuki K, Adachi M (1999) Preliminary CHIME dating of granites from the Nkambé area, northwestern Cameroon, Africa. J Earth Planet Sci 46:57–70

Tetsopgang S, Suzuki K, Njonfang E (2008) Petrology and CHIME geochronology of Pan-African high K and Sr/Y granitoïds in the Nkambe area, Cameroon. Gondwana Res 14:686–699

Tischendorf G (1977) Geochemical and petrographic characteristics of silicic magmatic rocks associated with rare-element mineralization. In: Stemprok M, Burnol L and Tischendorf G (eds) Metallization associated with acid magmatism, Czechoslovakia. Geological Survey, vol 3, pp 41–98

Toteu SF (1990) Geochemical characterization of the main petrographycal and structural units of northern Cameroon: implications for Pan-African evolution. J Afr Earth Sci 10:615–624

Toteu SF, Michard A, Macaudire J, Bertrand JM, Penaye J (1986) Données géochronologiques nouvelles (U/Pb et Rb/Sr) sur la zone mobile pan-africaine du Nord Cameroun (in French). Comptes Rendus D' Académique Des Science Paris, II 303:375–378

Toteu SF, Michard A, Bertrand JM, Rocci G (1987) U-Pb dating of Precambrian rocks from northern Cameroon, orogenic evolution and chronology of the Pan-African belt of central Africa. Precambrian Res 37:71–87

Toteu SF, Bertrand JM, Penaye J, Macaudière, J, Angoua S, Barbey P (1991) Cameroon: a tectonic keystone in the Pan-African network. In: Lewry JF, Stauffer MR (eds) The early proterozoic Trans-Hudson Orogen of North America. In: Special Paper 37. Geological Association of Canada, pp 483–496

Toteu SF, Van Schmus WR, Penaye J, Michard A (2001) New U–Pb and Sm–Nd data north-central Cameroon and its bearing on the pre-Pan African history of central Africa. Precambrian Res 108:45–73

Toteu SF, Penaye J, Poudjom Djomani Y (2004) Geodynamic evolution of the Pan-African belt in central Africa with special reference to Cameroon. Can J Earth Sci 41:73–85

Trompette R (1994) Geology of Western Gondwana (2000-500): Pan-African-Brasiliano Aggregation of South America and Africa. Balkema, Rotterdam

Van Lichtervelde M, Holtz F, Hanchar JM (2010) Solubility of manganotantalite, zircon and hafnium in highly fluxed peralkaline to peraluminous pegmatitic melts. Contrib Miner Pet 160:17–32

Wang XS, Gao J, Klemd R, Jiang T, Li JL, Zhang X et al (2017) The Central Tianshan Block: a microcontinent with a Neoarchean-Paleoproterozoic basement in the southwestern Central Asian Orogenic Belt. Precambrian Res 295:130–150

Wedepohl KH (1995) The composition of the continental crust. Geochim Cosmochim Acta 59:1217–1232

Whalen JB, Currie KL, Chappel BW (1987). A-type granites: Geochemical characteristics

Whitney DL, Evans BW (2010) Abbreviations for names of rock-forming minerals. Am Miner 95:185–187

Wolfe WJ (1977) Geochemical exploration of early Precambrian, volcanogenic sulphide mineralization in Ben Nevis Township, District of Cochrane. Ont Geol Surv 19:3

Yakeu SFA, Njanko T, Nzenti JP, Ganno S, Ngnotué T (2007) Évolution tectono-étamorphique de la région à l'ouest de Nkambé (province du Nord-Ouest Cameroun (in French). Notes Et Mémoire Service Géologie De Maroc 516:127–134

Yannah M (2020) Petrographical, geochemical and geophysical characterization of Somie-Ntem lithologies, Tikar plain, Cameroon: Implication for mineralization. Doctoral thesis, University of Dschang Cameroon

Yannah M, Suh CE, Mboudou MGM (2015) Quartz veins characteristics and Au mineralization within the Batouri Au District, East Cameroon. Sci Res 3:137–149

Yap L, Nouayou R, Tchaptchet Tchato D, Kamguia J, Bouba A (2018) Evidence for the upwelling of mafic bodies into the upper crust beneath the N40–50°E branch of the Pan-African Central Cameroon Shear Zone from Gravity Studies. Open J Geol 8:278–297

Zhao Y, Yang YQ, Ke JJ (2016) Origin of Cu- and Ni-bearing magma and sulfide saturation mechanism: a case study of Sr–Nd–Pb–S isotopic composition and element geochemistry on the Huangshannan magmatic Ni–Cu sulfide deposit, Xinjiang. Acta Petrologica Sinica 32:2086–2098